THE STUDY OF GROUND STATE AND EXCITED STATE PROPERTIES OF CYANINE DYES BY USING COMPUTATIONAL CHEMICAL METHODS

A Thesis Submitted to
the Graduate School of Engineering and Science of
İzmir Institute of Technology
in Partial Fulfillment of the Requirements for the Degree of

MASTER OF SCIENCE

in Chemistry

by
Sıla KARACA

July 2008
İZMİR

We approve the thesis of **Sıla KARACA**

_____

Assoc.Prof.Dr. Nuran ELMACI
Supervisor

_____

Prof.Dr. Serdar ÖZÇELİK
Committee Member

_____

Assoc.Prof.Dr. Cenk SELÇUKİ
Committee Member

9 July 2008

Date

_____

Prof.Dr. Hürriyet POLAT
Head of the Chemistry Department

_____

Prof.Dr. Hasan Böke
Dean of the Graduate School of
Engineering and Sciences

ACKNOWLEDGEMENT

I want to express my deepest gratitude to my supervisor Assoc. Prof. Nuran Elmacı, and I appreciate for her support, guidance, motivation and endless patience in this project. I could not have finished this thesis without her encouragement and instruction.

I also thank to Prof. Serdar Özçelik for inspirations to this study and help of the experimental part.

I wish also thank to Asst. Prof. Sami Sözüer, Inst. Hakan Kutucu and Koray Sevim to allow to use of their computational resources.

Also, I am indebted to İbrahim Karaman for his help in arrangement of the thesis.

Last but not least I would like to special thanks to my perfect family whose love is boundless Arife Karaca, Aysel Çermikli, Gönül Karaca Ucer, and Necmi Ucer for their love and endless support throughout my life.

ABSTRACT

THE STUDY OF GROUND STATE AND EXCITED STATE PROPERTIES OF CYANINE DYES BY USING COMPUTATIONAL CHEMICAL METHODS

The 5,5′,6,6′-tetrachloro-1,1′,3,3′-tetraethyl-benzimidazolo carbocyanine (TTBC) iodide, abbreviated $CBIC_2(3)$ or JC-1, is used for the molecular probe especially as measuring mitochondrial membrane potential and allows to visualize mitochondria, apoptosis or not.

The behaviors of the TTBC at the ground and excited states have been investigated by using quantum chemical methods. DFT/6-31G** levels of theory calculations have been carried out for the optimization and the frequencies with B3LYP and PBEPBE functionals for the ground state structure. TDDFT/6-31G** and CIS/6-31G** methods have been used for the excited state properties. In addition to those, solvation calculations were performed with CPCM and IEFPCM.

The effects of the functional groups, length of the conjugated chain, and alkyl groups on TTBC have been analyzed. There is no significant effect of functional groups either as donor or acceptor on the optimum structure. Only the alkyl groups change the planarity of the molecule. TTBC has a very rigid geometry. But it is possible to tune up λ_{max} with NH_2 and butyl/propyl and increasing polymethine chain length.

To explain the shoulder on the fluorescence spectrum, the PES section was obtained. The fluorescence property of TTBC was compared with the experimental data. Although perpendicular structure is favorable in the first excited state, there is no significant difference in dipoles. The twisted charge transfer state is absent in this dye based on these calculations. The solvent effect on TTBC in different solvents was investigated. The solvation calculations show that, λ_{max} values are independent of the polarity of the solvents as seen experimentally.

ÖZET

SİYANİN BOYALARININ TEMEL HAL VE UYARILMIŞ HAL ÖZELLİKLERİNİN HESAPLAMALI KİMYA YÖNTEMLERİYLE ÇALIŞILMASI

5,5′,6,6′-tetrakloro-1,1′,3,3′-tetraetil-benzimidazol-karbosiyanin (TTBC)-iyodür, (kısaca $CBIC_2(3)$ veya JC-1) özellikle mitokondri membran potensiyelini ölçmede moleküler prob olarak, mitokondriyi görüntüleyip hücre ölümünün olup olmadığını belirlemek amacıyla kullanılmaktadır.

TTBC'nin temel hal yapısı ve uyarılmış hal yapısındaki davranışları kuvantum kimyasal yöntemleri ile incelenmiştir. Temel hal yapısındaki optimizasyon ve frekanslar DFT/6-31G** teorisi B3LYP ve PBEPBE fonksiyonelleri ile hesaplanmıştır. Uyarılmış hal yapısı hesapları için TDDFT/6-31G** ve CIS/6-31G** metodları kullanılmıştır. Bunlara ek olarak çözücü etkisi hesapları CPCM ve IEFPCM ile hesaplanmıştır.

TTBC üzerindeki fonksiyonel grupların, konjuge zincirin uzunluğunun, ve alkil gruplarının etkisi incelenmiştir. Optimum yapı üzerinde elektron verici ve alıcı fonksiyonel grupların bile önemli etkisi olmamıştır. Sadece alkil gurupları molekülün düzlemselliğini değiştirmiştir. TTBC geometrisinin çok sıkı bir yapısı vardır. Ama λ_{max} değerini NH_2 ve butil/propil ve konjuge polimetin zincirini uzatarak artırmak mümkündür.

Floresans spektrumundaki omuzu açıklamak için potansiyel enerji yüzey kesiti elde edilmiştir. TTBC'nin floresans özelliği deneysel sonuçlarla karşılaştırılmıştır. Birinci uyarılmış halde 90^o dönmüş yapı tercih edilir olsa da, kayda değer dipol artması gözlenmemiştir. Bu hesaplamalara göre bükülmüş molekül içi yük transfer durumuna rastlanmamıştır. TTBC'nin farklı çözücülerdeki çözücü etkisi incelenmiştir. Hesaplamalar deneysel olarak da görülen λ_{max} değerinin çözücünün polaritesinden bağımsız olduğunu göstermiştir.

To my mother Arife Karaca;

Everything in my life…

TABLE OF CONTENTS

LIST OF FIGURES

Figure **Page**

LIST OF TABLES

Table **Page**

ABBREVIATIONS

AM1	Austin Model 1
B3LYP	Becke 3-Parameter (exchange), Lee, Yang and Parr (correlation)
B3PW91	Specifies this functional with the non-local correlation provided by Perdew/Wang 91.
CCSD(T)	Coupled-Cluster with Single and Double and Perturbative Triple Excitations
CD	Cis down
CI	Configuration Interaction
CIS	Configuration Interaction Singles
CIS1	CIS calculation with twisting angle from reaction coordinate (1) of TTBC
CIS2	CIS calculation with twisting angle from reaction coordinate (2) of TTBC
CISD	Configuration Interaction Single Double
COSMO	Conductor-like Screening Model
CPCM	Conductor-like Polarizable Continuum Model
CU	Cis up
D/A	Donor / Acceptor
DFT	Density Functional Theory
DMSO	Dimethylsulfoxide
DYEM	TTBC in Methanol Solvent
f	Oscillator Strength
HCTH	Handy's family functional including gradient-corrected correlation
HF	Hartree-Fock
HOMO	Highest Occupied Molecular Orbital
IEFPCM	Integral Equation Formalism Polarizable Continuum Model
INDO	Intermediate Neglect of Differential Overlap
JC-1	Another name of TTBC (5,5',6,6'-tetrachloro-1,1',3,3'-tetraethyl-benzimidazolo carbocyanine iodide)
LSDA	Local Spin Density Approximation
LUMO	Lowest Unoccupied Molecular Orbital

MINDO	Modified Intermediate Neglect of Differential Overlap
MNDO	Modified Neglect of Differential Overlap
MO	Molecular Orbital
MP2	Møller-Plesset Perturbation Theory 2
MP4	Møller-Plesset Perturbation Theory 4
MPW1PW91	Modified Perdew-Wang Exchange and Perdew-Wang 91 Correlation
NBO	Natural Bond Orbital
PBE1PBE	Hybrid Functional of Perdew, Burke and Ernzerhof
PBEPBE	Functional of Perdew, Burke and Ernzerhof
PES	Potential Energy Surface
PM3	Parameterization Method 3
PPP	Pariser-Parr-Pople
S0	Ground State
S1	First Excited State
S2	Second Excited State
SAM1	Semi-Ab-initio Model 1
STO	Slater Type Orbital
TD	Trans down
TD1	TDDFT calculation with twisting angle from reaction coordinate (1) of TTBC
TD2	TDDFT Calculation with twisting angle from reaction coordinate (2) of TTBC
TDDFT	Time-Dependent Density Functional Theory
TICT	Twisted Intramolecular Charge-Transfer
TTBC	5,5',6,6'-tetrachloro-1,1',3,3'-tetraethyl-benzimidazolo carbocyanine iodide
TU	Trans up
ZINDO	Zerner's Intermediate Neglect of Differential Overlap

CHAPTER 1

INTRODUCTION

1.1. Definition of Cyanine Dye

Cyanine dyes are synthetic dyes with the general formula $R_2N[CH=CH]_nCH=N^+R_2$ (*n* is a small number) in which the nitrogen and part of the conjugated chain usually form part of a heterocyclic system, such as imidazole, pyridine, pyrrole, quinoline and thiazole, etc. (IUPAC 2008).

Both of the nitrogens are bonded with the polymethine chain in the general formula. Cyanine dye is a non-systematic name and there are a lot of species according to their different R groups and polymethine groups in the literature.

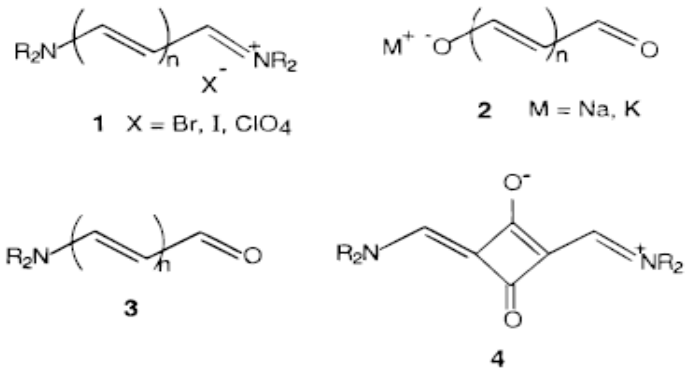

Figure 1.1. General structures of cyanine dyes
(Source: Mishra, et al. 2000)

Depending on the charge of the streptomethine unit, these dyes are classified as:

1. Cationic streptopolymethines cyanine and hemicyanine dyes
2. Anionic streptopolymethines oxonol dyes
3. Neutral streptopolymethines merocyanine dyes
4. Zwitterionic squaraine-based cyanine dyes

1.2. Application of Cyanine Dye

Cyanine dyes were first synthesized in the 1800s (Lakowicz 1994). They have various applications. Dyes are not used for only dying they are also used as sensitizers for photographic film such as cryptocyanine (Hamer 1964). Spectral sensitizers were extended to longer wavelengths for the visible or infrared spectrum.

They show high nonlinear optical properties owing to their wide transparent range, high nonlinear optical (NLO) coefficiency, large molecular hyperpolarizability (β), and short response time. Marder and co-workers studied the NLO properties of organic conjugated molecules and showed strong correlation between hyperpolarizability and bond-length alternation (BLA) in the conjugated bridge by using solvents of different polarity. The relationships between hyperpolarizability and BLA, Marder performed MO calculations with AM1 method (Mishra, et al. 2000).

Cyanines have been used as laser dyes (Maeda 1984) and antitumor agents (Kawakami, et al. 1998). They are ideal for fluorescent reagent. Their extinction coefficient is higher than 50,000 L/mol.cm and quantum yield of at least 5 percent. In addition to these, they can absorb and emit light maxima ranging from 400 nm to 900 nm. Cyanine and cyanine derivatives contain reactive groups. These reactive groups are covalently bonded to the component such as proteins, nucleic acids, cells, other biological and nonbiological materials, so components can be labeled an then to make these materials fluorescent so that they can be detected (Patent Storm 2005).

In one study, it has been shown that an iodoacetyl group of the cyanine dyes was used to form covalent bonds with sulfhydryl groups on the Sarcoplasmic Reticulum protein to activate Ca^{2+} release. So fluorescent dyes were used to label and isolate those proteins (Salama, et al. 1985).

Waggoner et al. investigated that the sulfhydryl group on rhodopsin has been covalently labeled with a cyanine dye having absorbance at 660 nm. Cyanine dyes are for labeling specifically the sulfhydryl group of a protein (Waggoner, et al. 1981). In these studies only specific cyanine dyes have an iodoacetyl group, which causes the cyanine dye to be covalently reactive with a sulfhydryl group on the proteins. But, the other materials do not have sulfhydryl groups and also many proteins do not have enough sulfhydryl groups to make fluorescence probing. Additionally, sulfhydryl groups are easily oxidized to disulfides in the presence of air. In this way it can not be

covalent binding to a fluorescence probe. Amine and hydroxyl groups are much more and more stable than sulfhydryl group in proteins and other materials. So larger cyanine dyes can attach to the component and high signal intensity will be given off (Patent Storm 2005).

Specific and selective cyanine dyes, which have different range of excitation and emission wavelengths, are very important to detect and distinguish the specific protein and the other materials. So the synthesis of different selective cyanine dyes is under development.

1.3. Introduction to Fluorescence Techniques

Fluorescence is the result of excitation, excited-state lifetime and fluorescence emission. A fluorescent probe is a fluorophore designed to localize within a specific region of a biological species. The fluorescence of fluorescent probes process is explained by the Jablonski electronic-state diagram (Haugland 2006).

Fluorescent probe dyes can be categorized into two groups (Reers, et al. 1991):

(1) Fast dyes with a response time to a change in the membrane potential of less than milliseconds.

(2) Slow dyes with a response time of seconds. Slow dyes, have found a wide field of application.

An ideal fluorescent probes properties must have;

- Characteristic absorption and emission wavelengths
- Conjugation with the component
- High light absorption
- High quantum yield
- Sensitivity

So cyanine dyes are ideal probes because they absorb and emit the light in the range of 400-900 nm and absorb light strongly, photostable, simple and effective coupling with the components, structure modification can be done, and can be bonded to the component easily according to the steric effect.

1.4. Optical Detection Methods

The detecting method can employ a light source. Such detection devices include fluorescence spectrometers, absorption spectrophotometers, fluorescence microscopes, transmission light microscopes and flow cytometers. Chemical analysis methods can also detect attachment of the dye to the labeled component. These methods can be infrared spectrometry, NMR spectrometry, absorption spectrometry, fluorescence spectrometry, mass spectrometry and chromatographic methods (Patent Storm 2005).

1.5. Dye Aggregation

Absorption of the dye can be changed at the different conditions. The dyes are different orientation in the solutions and aggregation can be occurred such as J-aggregates (a special type of multimer of carbocyanines that was first identified by Jelley, (Jelley 1937) or H-aggregates. So deviations from the Beer's law appearance and the maximum wavelength shift longer or shorter. The bathrochromically shifted (red shift) J-bands and the hypsochromically shifted (blue shift) H-bands according to molecule's orientation and effective of transition dipoles.

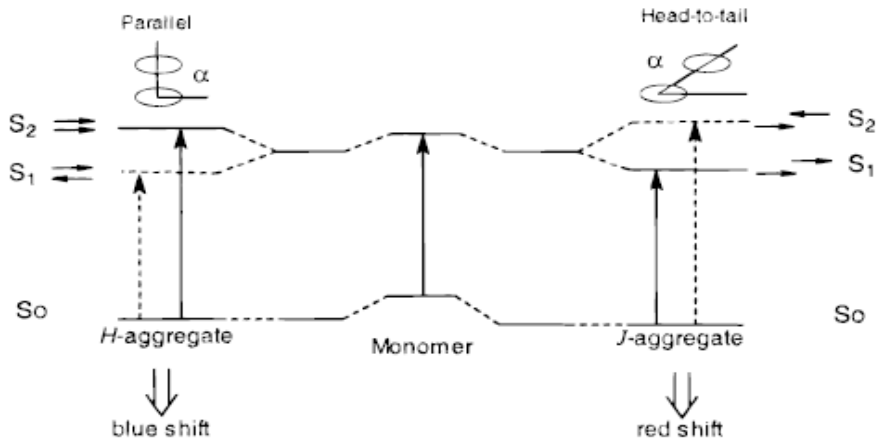

Figure 1.2. The relationship between chromophore arrangement and spectral shift based on the molecular exciton theory (Source: Mishra, et al. 2000)

The dyes aggregate in a parallel way (plane to plane) to form (sandwich-type arrangement) H-dimer or in head to tail (end to end) to form J-dimer. According to

Kasha's (McRae and Kasha 1958) point dipole approximation, if the angle α is less than about 54^o J-band formation occurs, if the α is greater than 54^o H-band formation occurs (Herz 1977).

Aggregation type of the dye depends on the structure and also on the environment, such as micellar, microemulsion, pH, ionic strength, concentration, solvent polarity, electrolyte, and temperature parameters. Generally, dye self-association in solution depends directly on dye concentration, added electrolyte and inversely on the temperature (Mishra, et al. 2000).

1.6. Photodimerization and Isomerization

Trans-cis isomerization is the important fundamental photoisomerization reaction. These experimental studies are investigated by flash photolysis, transient absorption, picosecond and femtosecond time-resolved spectroscopy. And also computational quantum chemical methods deal theoretically. So, experimental and computational methods help each other.

The trans-cis isomerisation is a reversible process. It depends on the twisting dihedral angle of the molecule around the double bond. When a molecule excited from the ground state. Geometry of the molecule can be changed so when emission occurred to the ground state. Trans or cis isomer can be formed by a thermal back reaction. The activation energy of the thermal back reaction depends on the steric affect, bond order and strength of the molecule. A model for the isomerization mechanism was studied firstly by Orlandi and Siebrand (Orlandi and Siebrand 1975) and Ruliere (Rulliere 1976).

The molecule is excited to the first excited singlet state as in the Figure 1.3. If the $E_{0,}$ the potential energy barrier is less, the molecule will overcome the barrier by the rate constant k_1. After that the trans or cis isomer can be formed in the ground state by the rate constant k_3. The height of the ground state potential curve is also important to thermal back reaction k_4 (Feller, et al. 1988).

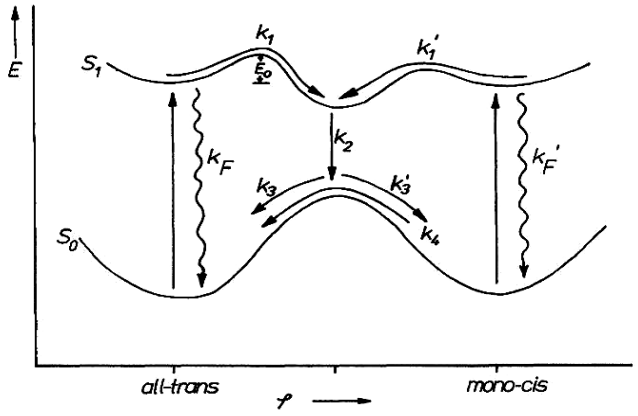

Figure 1.3. Excited state potential energy surface model
(Source: Feller, et al. 1988)

The potential energy surface diagram of the molecule is important for the rotating groups and the solvent molecules. The rotating groups are affected by the solvent molecules. The rate of the motion depends on the frictional forces of the various solvent parameter such as viscosity, polarity of the solvent etc. Sundström and Gillbro studied the dynamics of the radiationless relaxation of triphenylmethane (TPM) molecules in the *n*-alcohols methanol to octadecanol with picosecond absorption recovery techniques as a function of viscosity, temperature, and wavelength of the exciting and analyzing light. In going through the n-alcohol series the excited state potential surface changes from (E_0=0) in methanol to a surface having a potential barrier (E_0=15 kJ mol^{-1}) in the higher alcohols. So when polarity of the solvent decreases then potential barrier increases (Sundström and Gillbro 1984).

Rulliére's model (Rulliere 1976) assumes that a maximum energy exists in S_0 at $\theta=90^o$ (the perpendicular conformation) and minimum energy exist in S_1 when the reaction coordinate is rotating angle, θ. So the energy difference between S_0 and S_1 is minimum at $\theta=90^o$. This model is adapted to the photophysical behavior of carbocyanines (Rodriguez, et al. 1997).

Most of the cyanine dyes undergo photoisomerization. They have various applications such as in laser technology as Q switches and laser media, in photographic materials, in solar cells, in recording layer in compact disk (Nuernberger, et al. 2006). Generally all of the cyanine dyes have trans geometry in their stable form due to the energy of the molecule (Mishra, et al. 2000).

1.7. General Structure of TTBC

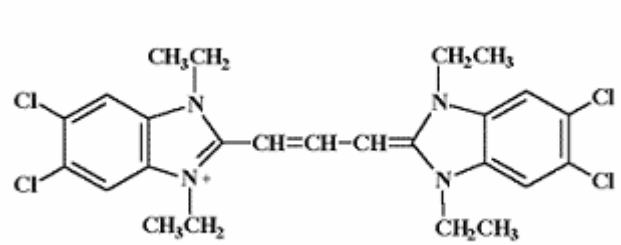

Figure 1.4. Cationic structure of TTBC

The chemical name 5,5′,6,6′-tetrachloro-1,1′,3,3′-tetraethyl-benzimidazolo carbocyanine iodide is abbreviated as $CBIC_2(3)$, another nomenclature is JC-1. The JC-1 stands for the first J-aggregate (Jelley, 1937) forming cationic dye.

JC-1 excited at 490 nm, the monomers emission maximum at 527 nm and J-aggregates with a broad excitation and a narrow emission spectrum at 590 nm. Cells with high mitochondrial ΔΨ fluorescence orange, and cells with low mitochondrial ΔΨ fluorescence green (Reers, et al. 1991).

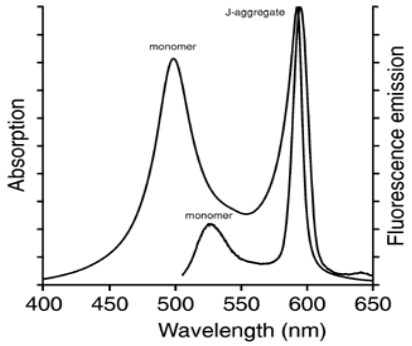

Figure 1.5. Absorption and fluorescence emission spectra of JC-1 pH 8.2 buffer containing 1% (v/v) DMSO (Source: Product Spectra 2008)

TTBC is a dye, which has a delocalized positive charge, used for the molecular probe especially as measuring mitochondrial membrane potential (ΔΨ) (Smiley, et al. 1991). Chen and Smiley described the properties of JC-1 and application in mitochondrial potentials in live cells (Chen and Smiley 1993).

It is known that mitochondria plays an important role in several biological processes, one of them is the cell death or apoptosis. For instance decreasing of the mitochondrial ΔΨ shows that apoptosis and JC-1 is at monomer form at this situation whereas increasing the mitochondrial ΔΨ shows that cell is alive and TTBC occurs in J aggregation form (Reers, et al. 1991).

1.8. Applications of TTBC (JC-1)

JC-1 is mainly used to detect apoptosis (Cossarizza and Salvioli 2001) and quantitative analysis of mitochondrial membrane potential (Huang, et al. 2007) to understand relationships between mitochondrial potential and intracellular calcium levels (Bowser, et al. 1998) as a selective target molecule for heat-shock related protection against oxidative stress (Polla, et al. 1996) and to find out mitochondrial myopathy as a defective function.

In a study, the sensitivity and specificity of three fluorescent probes were investigated, JC-1 is a reliable probe for investigating more specific for mitochondrial membrane potential (ΔΨ), and more consistent in its response to depolarization, than other cationic dyes such as DiOC6(3) and Rhodamine 123. The advantage of JC-1 over rhodamines and other carbocyanines is that its color changed reversibly from green to red with increasing membrane potentials. This provided the imaging live mitochondria on the stage of a microscope (Salvioli, et al. 1997).

Another mitochondrial marker, JC-9 (3,3'-dimethyl-α-naphthoxacarbocyanine iodide with similar potential-dependent spectroscopic properties. Although the green fluorescence of JC-9 is constant with membrane potential, but the red fluorescence is significantly increased at hyperpolarized membrane potentials (Haugland 2006).

In an experimental study, the steady state and the excited state properties of TTBC were investigated in different solvents. The stokes shift did not change with the orientational polarizability. Özcelik reported that the magnitude of the dipole moments in the excited state must be similar in the ground state and the electronic structure of the ground state is similar to the excited state structure (Ozcelik 2002).

1.9. Theoretical Studies on Cyanines

There are many combined experimental and theoretical studies on cyanine dyes. Optical properties of some cyanine dyes were investigated by using computational methods. Different levels of time dependent density functional theory (TDDFT) have been used to show the maximum of absorption of these dyes. As a consequence, excitation energies of these types of cyanine dyes can be predicted with good accuracy. And using integral equation formalism of the polarizable continuum model (IEFPCM), which include solvent effects, increasing the accuracy (Champagne, et al. 2006).

In another work, structure and absorption spectra for some cationic hemicyanine dyes with pyridine nucleus were investigated by using TDDFT-PCM model. The purpose of this study was the design of new hemicyanine dyes and to investigate the effect of the substituent groups. They used different DFT functionals and basis sets. Geometric parameters showed that these dyes with pyridine nucleus are planar conjugated molecules. The substituting groups affect the absorption spectra. The electron donor groups such as $N(CH_3)_2$, OH, OCH_3 or CH_3 attached to the dye increase the molecular conjugation. So λ_{max} became larger. In addition to attaching electron acceptor NO_2 in para position of the benzene ring increase the conjugation and λ_{max} is getting larger than the NO_2 in meta position due to the orbital population (Wang, et al. 2006).

Wang et al. performed a theoretical study on the structure and absorption properties of styrl dyes with quinoline nucleus with TDDFT method. They declared the changes of the ground and electronic structure with the different para and orto substituting groups. Consequently, the substituting groups, m-NO_2, p-Cl, p-OH, p-CH_3, p-OCH_3 or p-$N(CH_3)_2$ did not change the planar molecular skeleton. Furthermore highest occupied molecular orbital (HOMO) and lowest unoccupied molecular orbital (LUMO) are increased with the electron donor groups and decreased with the electron acceptor groups. The HOMO-LUMO energy gap reduced both electron acceptor and electron donor groups in meta-para substituted stryl dyes with quinoline nucleus. And electron donating groups make λ_{max} longer. TDDFT method gave theoretical λ_{max} values very similar to the experimental λ_{max} (Wang, et al. 2007).

Quantum chemical and spectral studies of the base derivatives of the symmetrical cyanine dyes have been examined recently. It was concluded that cationic

cyanine dyes have different equilibrium geometry, molecular orbital levels and electronic transitions than their bases. Experimentally, if the length of the polymethine group increases in dyes than cyanine dyes give high intensive and narrow spectral bands whereas their bases give wide spectral bands and also high intensive bands. λ_{max} of the cyanine dyes and bases is getting larger with increasing of the polymethine length (Kachkovsky, et al. 2006).

The potential energy surfaces for ground and excited states were obtained by Rodriquez group with quantum chemical methods, as a function of the rotating angle for six symmetric carbocyanines. The surfaces were calculated using Austin Model 1 (AM1) semiempirical quantum chemical model and excited state calculations were performed by Configuration Interaction (CI). Both experimental and calculated thermal back isomeration activation energy of the ground state decreases as increasing the polymethine chain length of the carbocyanine. And the calculation showed that the activation energy of the S_0 is larger than the S_1. In addition, the dipole moment shows a sharp peak at rotation angle $\theta=90^0$ (Rodriguez, et al. 1997).

Guillaumont and Nakamura worked on the ground state (S_0) and first excited singlet state (S_1) potential energy surfaces of different carbocyanines with the quantum chemical calculation. And photoisomer of carbocyanines lifetime was measured with the picosecond time-resolved fluorescence spectra. The isomerization potential energy surface affected with the length of the polymethine chain, its position on the quinoline moiety and the steric hindrance (Guillaumont and Nakamura 2000).

Rulliére was investigated the photoisomerization potential energy surface of the 3,3'-diethyloxadicarbocyanine iodide (DODCI). And it was concluded that when the twisting angle (θ) is 90^0 then S_0 state has the maximum energy whereas S_1 state has the minimum energy. The photophysical behavior of cyanine dyes, has been explained with this model widely. In another study ground state and first excited singlet state potential surfaces were obtained by a semiempirical method for the isomerization of symmetrical carbocyanines as a function of the twist angle around a carbon-carbon bond of the polymethine chain. They concluded that the isomerization potential surface depends on the polymethine chain length and steric hindrance has a significant role in the photoisomerization of carbocyanine (Park 2000).

Soujanya and co-workers studied the twisted intramolecular charge transfer phenomenon (Grabowski et al. 2003) for p-(N,N-dimethylamino) benzonitrile (DMABN) with the AM1 method. The ground and excited state profiles were

investigated against the rotating of angles and the photophysical properties of DBABN was showed (Soujanya, et al. 1995).

Very recently computational calculations were done on cyanine dyes, which are used in biomolecular detection (DNA and RNA), by rotating the torsinal angle of the dyes the fluoregenic properties of dyes and the effects of the position and the number of the fluorine atoms were investigated. Both semiempirical and ab-initio calculations were performed in this study. To understand the substituent effect on excitation energy, HOMO and LUMO gap was used. Finally, changing of the benzothiazole heterocycle with mono, para, di or tetrafluorobenzothiazole affect the reduction in aggregation and improve photostability (Silva, et al. 2007).

Bertolino group examined the solvachromic properties of indocyanine dyes by using the quantum chemical methods. The effect of the polymethine chain length and structure of the dyes were studied by Pariser-Parr_Pople (PPP) and TDDFT methods. The TDDFT method is successful for the effect of the solvent on the absorption wavelength of dyes and the effect of the solvents are linearly proportional with the refractive index (Bertolino, et al. 2006).

The spectra of the thioindigo dye derivatives were investigated by the TDDFT method. The effect of the solvent, cis trans isomerization and the chemical substitution on the benzene rings were analyzed and compared with the experimental results. As a result TDDFT found as a suitable method for quantitative predictions of the λ_{max} of the dyes. And the central double bond (C=C) lengths correlated of the color of substituted thioindigo, but C=O length and stretching frequency do not related with the λ_{max} (Jacquemin, et al. 2006).

Seth and Sean investigated the substituent effects of fluorescent protein chromophore anions with the twisted intramolecular charge-transfer (TICT) states. They claimed that proof of the importance of TICT states and charge-transfer intersections in the control of photoisomerization processes in fluorescent protein chromophores (Olsen and Smith 2007).

The discovery of dual fluorescence of p-(N,N-dimethylamino)benzonitrile (DMABN), was first discovered by Lippert (Lippert, Lüder, and Boos 1962). Many studies have been done on dual fluorescence. For instance a set of dual and nondual fluorescent molecules have been investigated by TDDFT method and the results are in agreement with experimental data. The calculations represented that the TICT model (Siemiarczuk, et al. 1977; Grabowski, et al. 1979) as a possible mechanism to illustrate

the dual fluorescence phenomenon and the potential energy surface is more significant than the geometrical structure to make reliable predictions about this model (Jödicke and Lüthi 2003).

The donor-acceptor substituted aromatic system's photophysical behavior was obtained and then compared with the theoretical results. The ground and excited states potential energy surfaces was performed both in vacuo and in acetonitrile as solvent using time dependent density functional theory and TDDFT polarized continum model (TDDFT-PCM) respectively. Results were predicted that a stabilized twisted excited state is responsible for red shifted charge transfer emission and the MO picture supports that the twisting along the donor part is responsible for the excited state CT fluorescence in molecule (Chakraborty, et al. 2006).

Gobbi et al. investigated the photophysical properties of N,N-dimethylaniline-(DMA) substituted tetraethynylethene (TEE; 3,4-diethynylhex-3-ene-1,5-diyne) and derivatives both in experimental and computational study. Experimental results showed that these molecules displayed dual flourescence depends on the solvent polarity. TICT model was offered to the dual flourescence with computational methods. In this study the stokes shift of the molecule and derivatives increased with the solvent polarity. In the computational part of the study, the molecules were rotated with different part of the bonds and then potential energy surface were calculated with the TDDFT method. Finally, they concluded that for rotation of the molecule was caused the singlet excited state shows minimum, a maximum for the dipole moment and oscillator strength was zero at the dihedral angle of twisting angle at 90^{o}. The decreasing of the oscillator strength and increasing with the dipole moment of the twisted conformation are characteristic of the TICT state (Gobbi, et al. 2001).

CHAPTER 2

COMPUTATIONAL METHODS

Computational chemistry is a branch of chemistry that expresses the properties of the molecules mathematically and solves them with computing skills. It allows chemists to investigate materials by running calculations on computer rather than experimentally. The calculations such as molecular energies and structures, molecular orbitals, multiple moments, atomic charges, electrostatic potentials, vibrational frequencies, spectroscopic properties, polarizabities, thermochemical properties and reaction pathways, etc.

There are two types of theory in the computational chemistry, molecular mechanics and electronic structure theory (Foresman and Frisch 1996). Molecular Mechanics use the laws of the classical physics on the other hand Electronic Structure Methods use the laws of quantum mechanics to investigate the properties of the molecules.

In the Molecular Mechanics, the calculations are not described in detail with the electrons. But it is based on the interactions among the nuclei. The data base of molecules used to a set of parameters and functions is called as a force field and computationally inexpensive method. To be used enormous atoms (thousands) such as proteins, DNA etc. (Foresman and Frisch 1996). One of the disadvantage of this method is that many chemical properties are not defined, such as electronic excited states. The other one is special force field is suitable only for a limited class of molecules.

In the Electronic Structure Method, the molecular properties can be solved by the Schrödinger Equation.

$$H\Psi = E\Psi \qquad (2.1)$$

where E is energy of the system, Ψ is the wavefunction, defines electron and nuclear positions and H is the Hamiltonian operator which includes both potential and kinetic energy.

Electronic Structure Methods can be classified into three groups these are Ab-initio, Semi-empirical and Density Functional Theory (DFT) methods.

For the ab-initio, semi-empirical and density functional methods brief explanations are given in the following sections since the details of these theories can be found easily from the most computational chemistry books. On the other hand the formulations for the TDDFT and the new solvation models will be described in more details.

2.1. Ab-initio Methods

The term ab-initio is Latin, means “from the beginning”. It calculates the properties of a system from first principles with no experimental parameters in their equations. The simplest type of ab-initio calculation is the Hartree-Fock (HF), an extension of molecular orbital theory, in which the correlated electron-electron repulsion is not specifically taken into account; only its average impact is included in the calculation.

Mostly ab-initio calculations give good results in the smaller molecules. Ab-initio methods are HF, MP2, CISD, MP4, CCSD(T), CCSDT, FULL CI (Young 2001). Any of the methods can be give the correct results. The disadvantage of the methods need powerful computer systems and large computational time in the calculations.

2.2. Semiempirical Methods

Semiempirical molecular methods use simpler Hamiltonian than the real Hamiltonian and use experimental data or results of the ab-initio calculations (Levine 2000). The methods are AM1, PM3, SAM1, INDO, MNDO, MINDO, ZINDO etc. The advantage of this method is much faster than the ab-initio methods and these methods are mostly good for molecular geometry and energy especially for organic compounds whereas semiempirical calculations give poor results for van der Walls and dispersion intermolecular forces because of the lack of diffuse basis functions. The other problem is the parameterization, if the calculated molecule is different from the experimental parameter so the results can be poor. Moreover, fewer properties can be predicted reliably in semiempirical calculations (Young 2001).

2.3. Density Functional Theory (DFT) Methods

Density Functional Theory does not use to the molecular wave function but use the molecular electron probability density ρ and molecular electronic energy from ρ in the calculations (Levine 2000). It is similar to ab-initio methods and it has become popular in recent years. Because effects of electron correlation was included in the calculations, the least expensive ab-initio method (Foresman and Frisch 1996).

Hohenberg & Kohn (Hohenberg and Kohn 1964) discovered that, the ground state density is enough to describe a stationary electronic system in 1964. The density is a very suitable variable: it is a physical observable, it has an intuitive interpretation, and it depends only on three spatial coordinates, however the many-body wave function, which is a complex function of 3N spatial coordinates. Hohenberg & Kohn also set up a variational principle in terms of the density (Marques and Gross 2004).

Kohn & Sham (Kohn and Sham 1965) proposed the use of an auxiliary noninteracting system called the Kohn-Sham system. The density of the interacting system is extracted from the the Kohn-Sham system. The electrons obey one-particle, Schrödinger equation with an effective external potential, v_{KS} within the Kohn-Sham system. The solution of this equation has to be obtained self-consistently as v_{KS} is a functional of the electronic density. The effective potential, v_{KS}, is partioned in to three terms,

$$v_{KS}(r) = v_{ext}(r) + v_{Hartree}(r) + v_{XC}(r) \tag{2.2}$$

The first term is the external potential which represent, the Coulomb interaction between the electrons and the nuclei, the second term includes the classical (Hartree) part of the electron-electron interaction. The last term is the unknown exchange-correlation (xc) potential, v_{xc}, which contains all the complex many-body effects. Kohn & Sham also suggested a simple approximation to v_{xc}, the local density approximation (LDA).

In summary, the basis of density functional theory (DFT) is the use of the density as the fundamental variable and the construction of the Kohn-Sham system. Density functionals can be categorized in various classes. One of them is the Xα, the simplest one, includes electron exchange not electron correlation. More complex set of functions uses the electron density and its gradient, which are called as gradient-

corrected methods. There are also hybrid methods that combine functionals of HF and other methods (Young 2001). Nowadays, the DFT results have been very good particularly for organic molecules.

2.4. Excited State Calculations

In the excited state calculations, energies and molecular properties of the molecule can be calculated. These calculations are used for the analysis of the spectroscopy, reaction mechanisms, etc.

A single excitation configuration interaction (CIS) calculation most usual way to obtain excited state calculations due to easy performing (Young 2001). It uses molecular orbitals that have been optimized with a HF calculation. The CIS calculation of the vertical excitation energy is obtained from the difference between the excited state energy found as a root of a secular equation and the ground state energy (Levine 2000). Each of the excited state geometries can be optimized and also vibrational frequencies can be calculated.

Recently, the time-dependent density functional theory (TDDFT) has a wide popularity in quantum chemistry. It is a useful tool for obtaining electronic excited state energies. TDDFT can be considered as an exact reformulation of time-dependent quantum mechanics, where the fundamental variable is the density but not the many-body wave function (Marques and Gross 2004).

The original TDDFT was founded by Runge & Gross (Runge and Gross 1984). based on the derivation of Hohenberg-Kohn–like theorem for the time-dependent Schrödinger equation. in 1984.The application of this formalization of DFT included generally the interaction of electromagnetic fields with matter.

The nonrelativistic time dependent many-body Schrödinger equation: is

$$i\frac{\partial}{\partial t}\Psi(\{r\},t) = \hat{H}(\{r\},t)\Psi(\{r\},t) \tag{2.3}$$

where $\hat{H}$ is the Hamilton operator of the system and $\{r\} = \{r_1,.....,r_N\}$ are the spatial coordinates of the N electrons.

The Hamiltonian is divided into three parts;

$$\hat{H}(\{r\},t) = \hat{T}(\{r\}) + \hat{W}(\{r\}) + \hat{V}_{ext}(\{r\},t) \tag{2.4}$$

The first two are the kinetic energy and the electron-electron interaction,

$$\hat{T}(\{r\}) = -\frac{1}{2}\sum_{i=1}^{N}\nabla^2{}_i \tag{2.5}$$

$$\hat{W}(\{r\}) = \frac{1}{2}\sum_{\substack{i,j=1 \\ i\neq j}}\frac{1}{|r_i - r_j|} \tag{2.6}$$

The third term can be written as a sum of one-body potentials,

$$\hat{V}_{ext}(\{r\},t) = \sum_{i=1}^{N} v_{ext}(r_i,t) \tag{2.7}$$

The electronic density n(r,t) is the basic variable of TDDFT. The central theorem of TDDFT proves that there is a one-to-one correspondence between the external (time-dependent) potential, $v_{ext}(r, t)$, and the electronic density, for many-body systems evolving from a fixed initial state. Kohn-Sham electrons obey the time-dependent Schrödinger equation;

$$i\frac{\partial}{\partial t}\varphi_i(r,t) = \hat{H}_{KS}(r,t)\varphi_i(r,t) \tag{2.8}$$

where the Kohn-Sham Hamiltonian is defined as

$$\hat{H}_{KS}(r,t) = -\frac{\nabla^2}{2} + v_{KS}[n](r,t) \tag{2.9}$$

The density of the interacting system can then be calculated from the Kohn-Sham orbitals

$$n(r,t) = \sum_{i}^{N} \left|\varphi_i(r,t)\right|^2 \tag{2.10}$$

As in the Kohn-Sham scheme for the ground state, the time-dependent Kohn-Sham potential is given as,

$$v_{KS}[n](r,t) = v_{ext}(r,t) + v_{Hartree}[n](r,t) + v_{XC}[n](r,t) \tag{2.11}$$

The first term denotes the external potential, the second refers to the classical electrostatic interaction between the electrons. The last term, the exchange, xc potential, which contains all nontrivial many-body effects, and has an extremely complex (and essentially unknown) functional dependence on the density.

It is important to point out that, like in ground-state density functional theory, the approximation to the xc potential which is the only fundamental approximation in TDDFT signify the quality of the results (Marques and Gross 2004). Casida used response theory for a TD-DFT molecular algorithm in 1995. Then calculations of different response properties of fairly large molecules up to hundreds of atom become possible.

In recent times TDDFT linear response theory become the most widely used electronic structure method for calculating vertical electronic excitation energies. Except for well-known problems such as, charge transfer (Casida, et al. 2000), Rydberg states (Hirata, et al. 2003) and double excitations (Hirata and Gordon 1999; Grotendorst, Blügel and Marx 2006). The linear response states of TDDFT consist of single excitations from the Kohn-Sham reference determinant, the computational cost is comparable to Hartree-Fock based single excitation methods, such as configuration interaction with single excitations (CIS). The electron correlation is correctly treated in principle, excitation energies compared to CIS methods (Ko, et al. 2008).

2.5. Solvent Effects

Gas phase calculations are usually insufficient for describing the behavior of many molecules in solution. In gas phase it is assumed that there is not any interaction with other molecules. The properties of molecules and transition states can differ

between the gas phase and solution. However, most of the chemistry occurs in solution. Hence solvents play an important role on the systems (Foresman and Frisch 1996).

When a solute is added to the solvent then its charge distribution interacts with the solvent. The addition of solute molecules to the solvent induces the dipole moment of solvent molecules around them. The solvent gains a polarization in the region of each solute molecule as a result of induction and the orientation of solute molecules. The polarized solvent produce an electric field is called the reaction field at each solute molecule (Levine 2000). The continuous electric field is used instead of the charge distribution in a continuum model. A solute is treated as a general charge density ρ in a cavity of general shape within a solvent which is taken as a continuous medium with permittivity ε. The field in the regions of space occupied by the solute is defined as reaction field.

All continuum solvent models depend on the Poisson equation which is based on the classical electrostatics (Cramer 2002). The electrostatic potential V, which is a function of charge density, ρ, and the permittivity, ε, has to satisfy the Poisson equation (Sharp and Honig 1990):

$$-\vec{\nabla}.(\varepsilon(\vec{r})\vec{\nabla}(\vec{r})) = 4\pi\rho(\vec{r}) \qquad (2.12)$$

where r is the position vector. In continuum solvation, the solute is represented explicitly and the solvent implicitly. It is thought that the charge distribution of the solute is inside a cavity within a homogeneous dielectric field. There are two regions as inside and outside the cavity.

The shape and size of the cavity are different depending on the continuum models. There is no unique definition of molecular cavity. There are three surface definition to define the shape of the cavity, Van der Waals (VDW) surface (VWS) (Figure 2.2) which is constructed from the overlapping VDW spheres of the atoms, the solvent accessible surface (SAS) (Figure 2.1), is the surface traced by the center of the probe sphere(solvent molecule) as it rolls on the VdW surface and the solvent excluded surface (SES) (Figure 2.1), that is topological boundary of the combination of all possible probes that do not overlap with the molecule (Tomasi, et al. 2005).

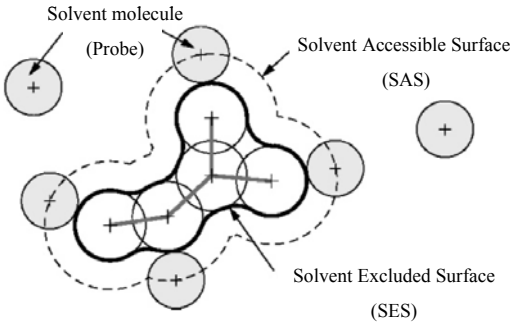

Figure 2.1. Solvent accessible surface (SAS) and solvent excluded surface (SES) (Source: Tomasi, et al. 2005)

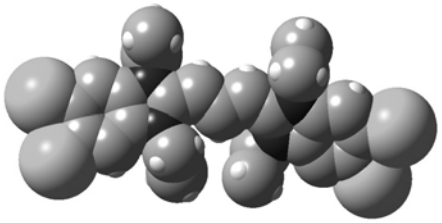

Figure 2.2. Van der Waals surface (VWS) of TTBC

The Poisson equation is used when there is no ionic strength. If there is a mobile electrolyte the Poisson-Boltzman equation is valid which introduces the effects of ions using the Debye-Huckel theory (Sharp and Honig 1990).

$$-\vec{\nabla}.(\varepsilon(\vec{r})\vec{\nabla}(\vec{r})) + \kappa'^2 \sinh[V(\vec{r})] = 4\pi\rho(\vec{r}) \qquad (2.13)$$

where the inverse of κ is Debye-Huckel length is related to the ionic strength I, N_a is Avogadro's number, k is the Boltzman constant and T is the temperature.

$$\kappa^2 = \frac{\kappa'^2}{\varepsilon} = \frac{8\pi N_a e^2 I}{1000\,\varepsilon kT} \qquad (2.14)$$

Although it is possible to solve the Poisson-Boltzman equation analytically for simple geometries, for complex geometries the solutions can be obtained numerically.

The molecular electronic wave function and all molecular properties in solution will be different than in gas phase. In the usual quantum mechanical implementation of the continuum solvation model, the electronic wave function and the electron probability density of the solute molecule are allowed to change on going from the gas phase to the solution phase so as to achieve self consistency between the solute molecule charge distribution and the solvents reaction field. Any treatment in which

such self consistency is achieved is called as self consistent reaction field (SCRF) model (Levine 2000).

The solute-solvent electrostatic interactions V^R defined by a proper quantum mechanical operator on the cavity surface depends on the solute charge density (ρ),

$$V^R(\rho) = \sum_k q(s_k;\rho)V(s_k) \tag{2.15}$$

where s_k shows point of tessera k, which is the division of the cavity surface into N finite elements, at which the charge q_k.

The Schrödinger equation with effective Hamiltonian, H^{eff} is,

$$H^{eff}\Psi^S = \left[H^0 + V^R\right]\Psi^S = E^S\Psi^S \tag{2.16}$$

where H^0 is gas phase Hamiltonian, Ψ^s is the polarized wavefunction and E^s is the eigenvalue in SCRF.

The most widely used method for self consistent reaction field implementations of the Poisson equation is polarized continuum model (PCM) formalized by Miertus, Scrocco, and Tomassi in 1981 (Miertus, et al. 1981). PCM uses apparent surface charge approach. Solute is placed in a cavity and an apparent charge on the cavity surface. The reaction potential is defined by introducing an apparent surface charge density (σ) on the cavity.

There are several models of PCM, characterized by the particular choice of electrostatic boundary conditions, Dielectric PCM (DPCM) (Cossi and Barone 1998) and Integral equation formalism PCM (IEFPCM) (Menucci, et al. 1997; Menucci and Tomassi 1997; Cansés, et al. 1997) and the conductor-like PCM (CPCM) (Barone and Cossi 1998; Cossi, et al. 2003). Among these methods, IEFPCM is the most general because it can model with consistent accuracy not only isotropic solvents with both high and low dielectric constant but also non-isotropic and ionic solutions. In IEFPCM formalism, the proper Green functions, defined inside and outside the cavity are used to evaluate the integral operators defining the apparent charge (Scalmani, et al. 2006).

2.6. Aim of The Study

The purpose of this study is to investigate the ground and excited state behaviors of the well known mitochondria selective cyanine dye TTBC (JC-1) by the use of quantum chemical methods. In this work an experimental study of the absorption and fluorescence property of TTBC was compared with the computational work. The effects of functional groups on the benzimidazole rings, length of the conjugated chain, and alkyl groups bonded to the nitrogen atoms have been analyzed. We hoped that with the help of this study the properties of the TTBC at the ground and excited state could be determined easily and will give insight to the design of the synthesis of new dye derivatives.

CHAPTER 3

RESULTS

3.1. Optimization Part of TTBC

The calculations were performed by Gaussian03 (Frisch et al 2003) and the visualization parts were done with GaussView 3.0 program. The B3LYP/6-31G** level of theory was chosen in our optimizations at the beginning of the study since it is well known for similar molecules. Later with the access of new computational resources, the other methods were also performed to validate the level of calculation. TTBC was optimized with different levels of theory. Table 3.1 shows the deviations from the X-Ray data; ($\Sigma(x_{cal}-x_{xray})^2$) for some critical bond lengths and angles) (Smith and Luss 1972). The iodide ion (counter ion) of the TTBC ignored in the calculations.

Table 3.1. Deviations from the X-Ray data of TTBC

Calculated vs Xray Data	dyem*	$dyem_a$
AM1	38.4	36.2
PM3	15.3	16.8
PBEPBE/6-31+G**	5.5	18.7
HF/3-21G**	8.5	12.5
HF/6-31G**	7.2	8.6
HF/6-311G**	7.2	8.1
B3LYP/3-21G**	6.5	9.8
B3LYP/6-31G**	5.8	6.3
B3LYP/6-311G**	6.5	6.7
PBEPBE/6-31G**	5.0	5.8
PBE1PBE/6-31G**	4.1	5.6
LSDA/6-31G**	2.8	10.2
STO-3G	5.5	6.4

*dyem refers to X-Ray data of TTBC dye in methanol and subscript $_a$ refers to the calculations in which atom labels are taken in the reverse order.

Overall observations showed that average errors of dyem and $dyem_a$ are about 5-6 units for the last six calculations in Table 3.1. On the basis of this, DFT/B3LYP/ 6-31G** level of theory was suitable for the optimization part, because it is successful and most widely used method in similar dye molecules (Wang, et al. 2007).After the method was selected the ground state properties such as bond lengths , angles, charges and frontier orbitals, etc. were investigated. The bond lengths and angles of TTBC are displayed in Figure 3.2 and Figure 3.3 respectively. The bond lengths along the backbone are about 1.400 A^o which is in between single and double bonds of carbon, that reflects the conjugation on the molecular plane.

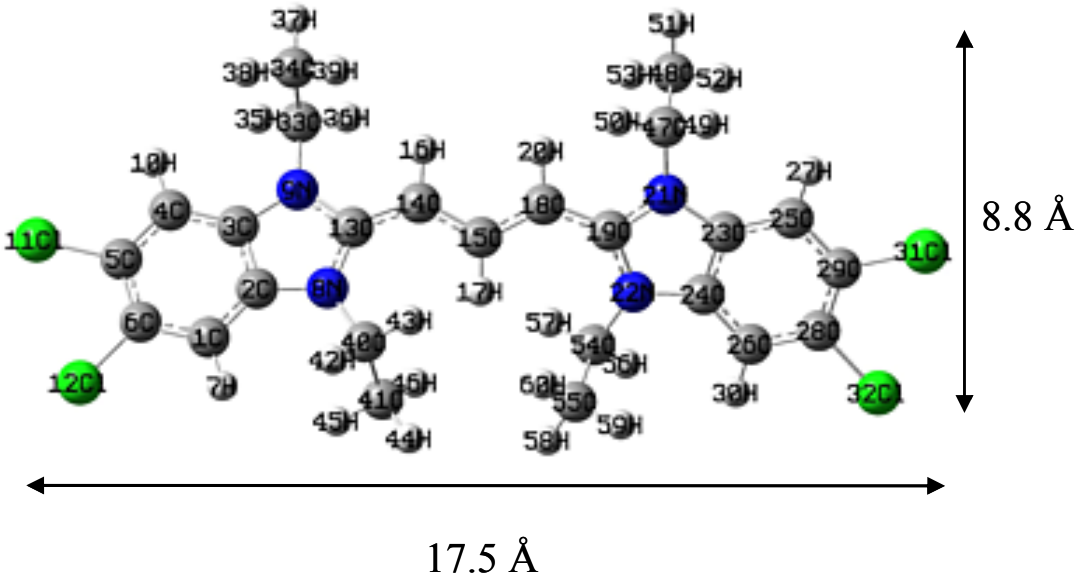

Figure 3.1. Structure of TTBC

The size of the TTBC is about 17.5 A^o x 8.8 A^o (Figure 3.1) (X-ray Length=17.39 A^o in DYEM) and deviation from the planarity, the angle of the two rings, is 19.6^o (X-ray angle =4.0 ^{o}). The comparison between calculated geometrical parameters and experimental data is given in Table 3.2. There is a positive error of about 16, this may be explained with the packing effect in crystal.

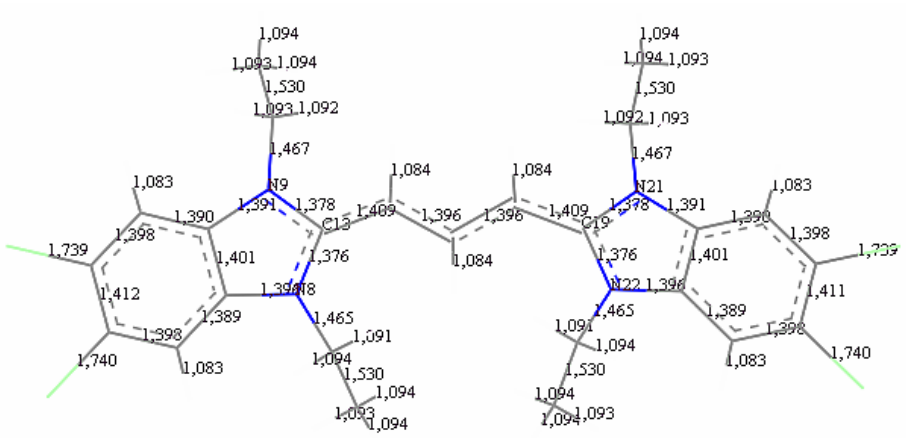

Figure 3.2. Bond lengths of TTBC

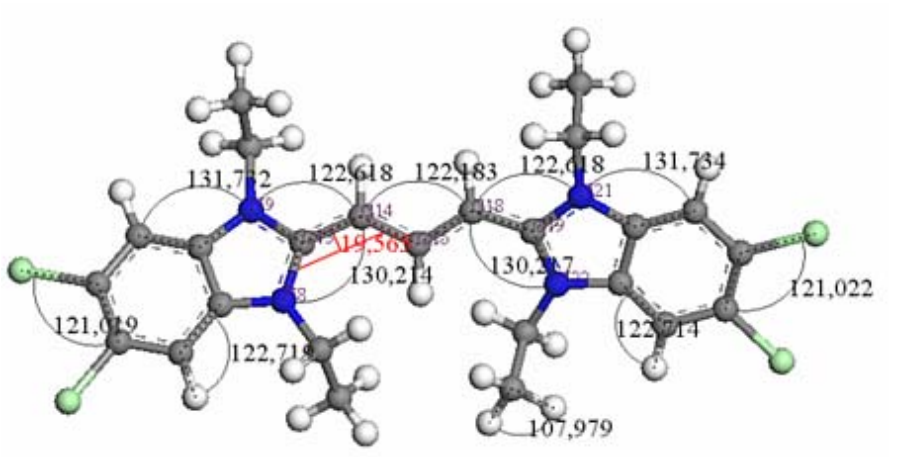

Figure 3.3. Bond angles of TTBC

Table 3.2. Some selected bond lengths and angles of TTBC

Bond Lengths(Å)

Atoms	B3LYP/ 6-31G**	X-RAY DYEM [a]
C1-C2	1.389	1.374
Cl11-C5	1.739	1.737
C6-C5	1.412	1.388
C13-N9	1.378	1.372
C13-N8	1.377	1.364
N9-C3	1.391	1.388
N8-C2	1.396	1.393
C15-C14	1.396	1.380
C14-C13	1.409	1.394

Bond Angles(°)

Atoms	B3LYP/ 6-31G**	X-RAY DYEM [a]
N9-C33-C34	113.1	112.7
N9-C13-N8	107.1	107.2
Cl11-C5-C6	121.0	119.5
Cl11-C5-C4	118.0	118.2
N9-C3-C4	131.7	131.0
N8-C2-C1	131.4	131.3
C15-C18-C19	129.9	129.0
C13-C14-C15	129.9	129.5
C14-C13-N8	130.2	130.8
N8-C13-C14-C15	19.6	4.0

Table 3.3. The Mulliken and Natural Bond Orbital (NBO).charge distributions of TTBC

		Mulliken	NBO			Mulliken	NBO			Mulliken	NBO
1	**C**	-0.085	-0.265	**21**	**N**	-0.609	-0.369	**41**	**C**	-0.327	-0.705
2	**C**	0.313	0.152	**22**	**N**	-0.620	-0.376	**42**	**H**	0.148	0.260
3	**C**	0.325	0.155	**23**	**C**	0.325	0.155	**43**	**H**	0.137	0.254
4	**C**	-0.084	-0.263	**24**	**C**	0.313	0.152	**44**	**H**	0.138	0.256
5	**C**	-0.110	-0.062	**25**	**C**	-0.084	-0.263	**45**	**H**	0.141	0.253
6	**C**	-0.111	-0.064	**26**	**C**	-0.085	-0.265	**46**	**H**	0.121	0.234
7	**H**	0.136	0.272	**27**	**H**	0.140	0.274	**47**	**C**	-0.086	-0.269
8	**N**	-0.620	-0.376	**28**	**C**	-0.111	-0.064	**48**	**C**	-0.324	-0.705
9	**N**	-0.609	-0.369	**29**	**C**	-0.110	-0.062	**49**	**H**	0.145	0.259
10	**H**	0.140	0.274	**30**	**H**	0.136	0.272	**50**	**H**	0.141	0.257
11	**Cl**	0.061	0.063	**31**	**Cl**	0.061	0.063	**51**	**H**	0.142	0.259
12	**Cl**	0.059	0.061	**32**	**Cl**	0.059	0.061	**52**	**H**	0.138	0.250
13	**C**	0.589	0.464	**33**	**C**	-0.086	-0.269	**53**	**H**	0.127	0.241
14	**C**	-0.186	-0.404	**34**	**C**	-0.324	-0.705	**54**	**C**	-0.090	-0.266
15	**C**	-0.022	-0.155	**35**	**H**	0.145	0.259	**55**	**C**	-0.327	-0.705
16	**H**	0.099	0.249	**36**	**H**	0.141	0.257	**56**	**H**	0.148	0.260
17	**H**	0.086	0.223	**37**	**H**	0.142	0.259	**57**	**H**	0.137	0.254
18	**C**	-0.186	-0.404	**38**	**H**	0.138	0.250	**58**	**H**	0.138	0.256
19	**C**	0.589	0.464	**39**	**H**	0.127	0.241	**59**	**H**	0.141	0.253
20	**H**	0.099	0.249	**40**	**C**	-0.090	-0.266	**60**	**H**	0.121	0.234

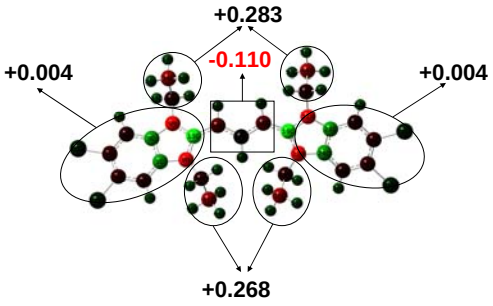

Figure 3.4. Mulliken charges of TTBC

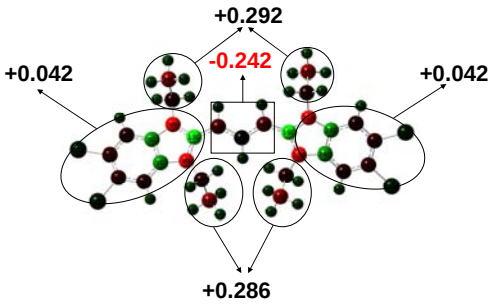

Figure 3.5. NBO charges of TTBC

The Mulliken and NBO atomic charges are given in Table 3.3. For the charge analysis the molecule was divided into seven groups. The groups are two benzimidazoles, four alkyls and one polymethine chain. The charges of these groups are shown in Figure 3.4 and Figure 3.5 in color scale. The color scale changes from red to green which means from most negative to most positive. The alkyl groups are carrying all positive charges while polymethine chain is negatively charged and the benzimidazole rings have almost zero charge according to both Mulliken and NBO analysis. But the magnitudes of the charges are different. Alkyl groups have similar

charges in both methods however the charge on polymethine chain is almost doubled in NBO.

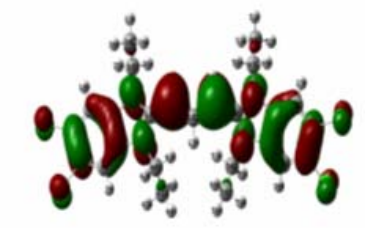

Figure 3.6. HOMO of TTBC

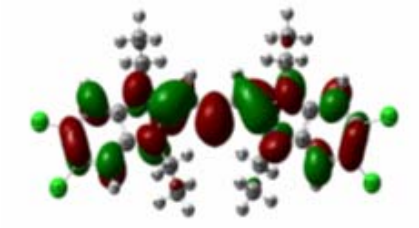

Figure 3.7. LUMO of TTBC.

There is no electron distribution on the ethyl groups and the electrons spreads out on the backbone of the molecule. The HOMO-LUMO pictures shows that the electrons are migrated from Cl atoms to the molecule **(**Figure 3.6 and Figure 3.7). Chlorine atoms act as electron donor. HOMO has π and LUMO has π^* character.

3.2. Side Group Effect on the TTBC

In the second part of the study, the effects of functional groups substituted the benzene rings, length of the conjugated chain, and alkyl-groups bonded to the nitrogen atoms on the ground and excited state properties of the TTBC have been analyzed via quantum chemical methods.

Geometry optimizations and frequency calculations were performed with DFT/B3LYP/6-31G(d,p) level of theory. The frequencies were checked for imaginary frequencies. No negative frequencies were found for all optimizations which state that all structures are minimum. The first fifteen vertical singlet excited states were computed by using TDDFT/B3LYP/6-31G(d,p) on the optimized geometries. The highest oscillator strength points out the most intense peak in the spectrum.

3.2.1. Effect of Donor-Acceptor Side Groups

The R Groups of the molecule were changed as shown in Figure 3.8 and with the activating functional group attached to a benzene molecule that gives electron density to the benzene ring, making electrophilic aromatic substitution reactions faster than benzene or a deactivating group which is a functional group attached to a benzene

molecule that removes electron density from the benzene ring, making electrophilic aromatic substitution reactions slower than benzene (Table 3.4).

Table 3.4. Activating and deactivating groups

Strongly Activating Groups	Strongly Deactivating Groups
$-NH_2$, -NHR, $-NR_2$, -OH, -O-	$-NO_2$, $-NR_3^+$, $-CF_3$, CCl_3
Moderately Activating Groups	Moderately Deactivating Groups
$-NHCOCH_3$, -NHCOR, $-OCH_3$, -OR	-CN $-SO_3H$ $-CO_2H$, $-CO_2R$,-COH, -COR
Weakly Activating Groups	Weakly Deactivating Groups
$-CH_3$, $-C_2H_5$, -R, $-C_6H_5$	-F, -Cl, -Br, -I

Cyanine dye derivatives with different functional groups R_1, R_2, R_3, R_4 are shown Figure 3.8 and Table 3.5.

Table 3.5. Cyanine dye derivatives with different side groups

	R_1	**R_2**	**R_3**	**R_4**
1R	**R**	H	H	H
2R	**R**	**R**	H	H
3R	**R**	**R**	**R**	H
4R	**R**	**R**	**R**	**R**
CD	**R**	H	**R**	H
CU	H	**R**	H	**R**
TD	**R**	H	H	**R**
TU	H	**R**	**R**	H

CD=cis down; CU= cis up; TU= trans up; TD= trans down; The abbreviations were given according to four ethyl groups. Ethyl groups bonded to N9 and N22 atoms are in up position whereas they bonded to N8 and N21 atoms are in down position from the molecular plane (Figure 3.1).

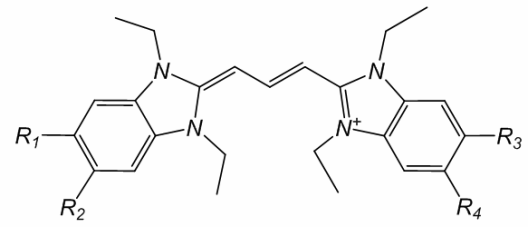

Figure 3.8. Cyanine dye derivatives with different side groups

Table 3.6. Dihedral angle of N8-C13-C14-C15 and the bond lengths of C5-C6 for 4R

4R→	NH_2	OCH_3	CH_3	Cl	CN	NO_2
D.Angle	24.34	20.98	20.32	19.57	18.91	18.94
B.L(C5-C6)	1.430	1.428	1.422	1.412	1.423	1.404

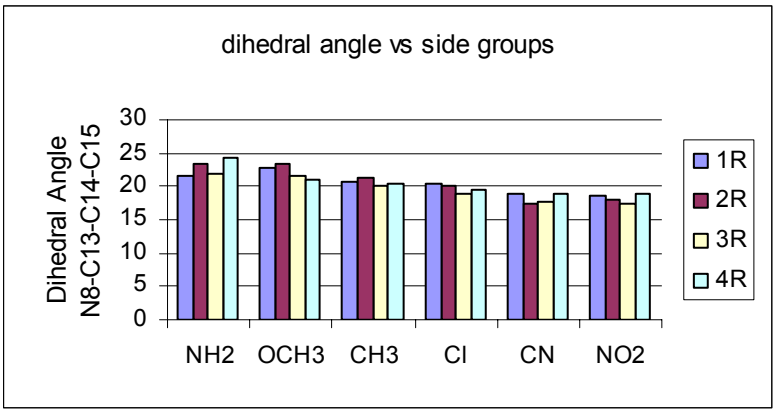

Figure 3.9. Dihedral angles of the dye with different side groups

Dihedral angles (N8-C13-C14-C15) decrease from donor groups to acceptor groups slightly. The largest difference of the angle is in between -NH_2 and -NO_2 groups about 5^o. So adding of the activating and deactivating groups do not impact the planarity of the molecule. The bond lengths of the molecule are almost the same. The most affected bond length was decreased from donor to acceptor groups about 0.03Å except for –CN group (Table 3.6).

The Mulliken atomic charges are given in Table 3.7 for groups shown in Figure 3.10. When compared to JC-1 (TTBC), electron donor moieties increased the charge on benzimidazole rings but decreased the charge on the rest of the molecule. The opposite case is observed for the acceptor groups.

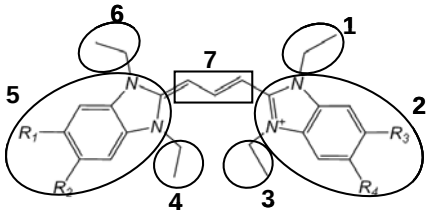

Figure 3.10. Charge groups on cyanine dye derivatives with different side groups.

Here, division of the molecule into seven groups was demonstrated.

Table 3.7. Mulliken charges of 4R

4R→ Group no	NH_2	Cl	NO_2
1	0.261	0.283	0.302
2	0.075	0.004	-0.050
3	0.247	0.268	0.287
4	0.247	0.268	0.287
5	0.075	0.004	-0.050
6	0.261	0.283	0.302
7	-0.161	-0.110	-0.079

When we add only one donor/acceptor (D/A) (1R) unit, the most effected group is the benzimidazole ring to which the R group attached becomes more positive/negative compared to Cl substituted dye (Figure 3.11). If two D/A (2R) added to the same ring then the same effect is observed more strongly (Figure 3.12). On the other hand if 3 D/A (3R, 2 in the same ring) are joined to the molecule in addition to benzimidazole rings, alkyl groups near to the 2D/A attached ring are slightly effected too (Figure 3.13). As can be seen in Figure 3.14 when all of the side groups (4R case) are acceptors then the benzimidazole groups (2 and 5) becomes negative but still most close to zero, ethyl groups is (1, 3, 4, 6) are more positive and chain (7) less negative but when the side groups are donors then benzimidazole groups are more positive, ethyl groups are less positive and chain is more negative with respect to the TTBC molecule.

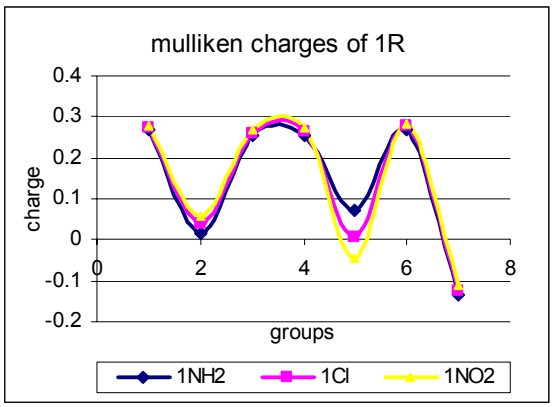

Figure 3.11. Mulliken charges of 1R

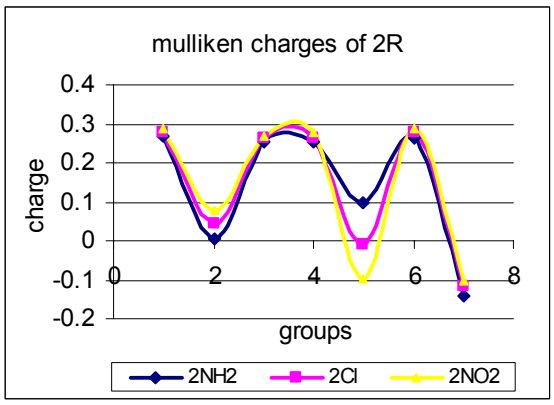

Figure 3.12. Mulliken charges of 2R

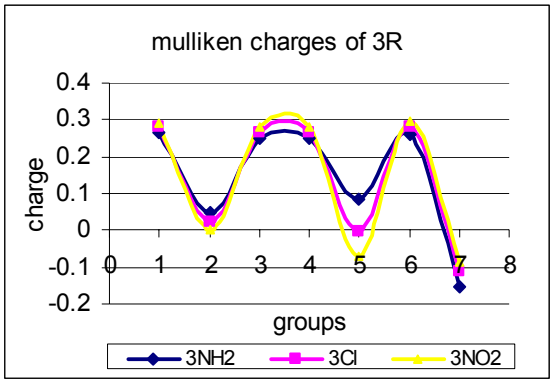

Figure 3.13. Mulliken charges of 3R

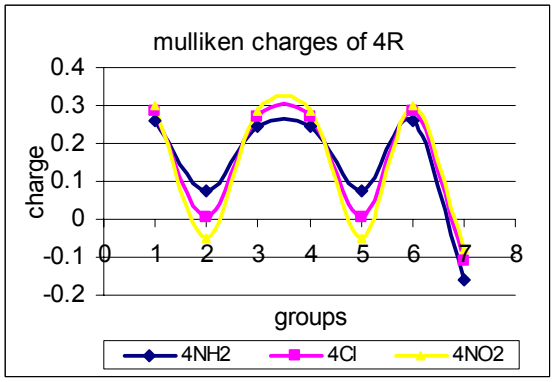

Figure 3.14. Mulliken charges of 4R

In Figure 3.15 the dipole moments of dye derivatives show that the donor groups play minor role whereas the effect of the dipole moment for the acceptor groups are larger. It changes according to their number of bonded groups and increases from Cl to NO_2 between the acceptor groups. The most effected dipole moment has been observed for the two acceptor substituted benzimidazole group and the least effected one is observed in 4R derivatives. This can be explained with the symmetry of the dye derivatives. In 4R acceptors the molecule is symmetric, so dipole vectors almost cancel each other, whereas in 2R acceptors on the same side the molecule is asymmetric and large dipoles are appeared.

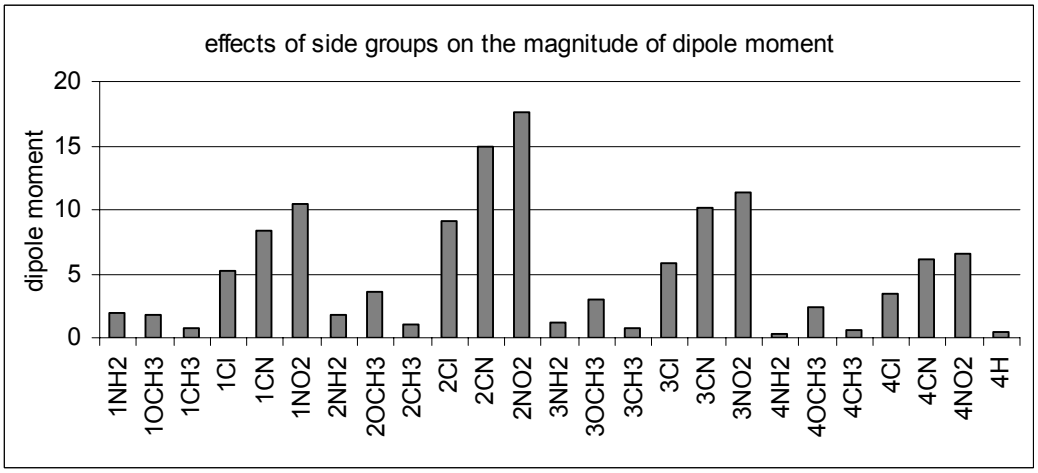

Figure 3.15. Dipole moments of 1R, 2R, 3R, 4R

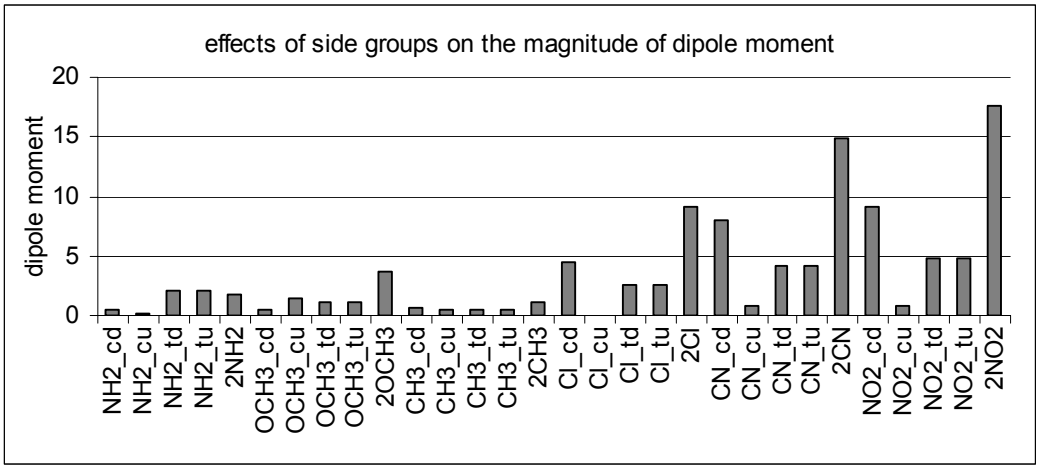

Figure 3.16. Dipole moments of 2R isomers

The dipole moments of the donor groups were not affected by the region but the acceptor groups are regio-sensitive (Figure 3.16).

Table 3.8. HOMO-LUMO energies of 4R

4R→	$4NH_2$	$4OCH_3$	$4CH_3$	4Cl	4CN	$4NO_2$
E_{LUMO} (eV)	-0.139	-0.150	-0.152	-0.176	-0.203	-0.206
E_{HOMO} (eV)	-0.244	-0.258	-0.265	-0.287	-0.313	-0.316
E_{LUMO} - E_{HOMO}	0.105	0.108	0.113	0.111	0.110	0.110

Both HOMO and LUMO energies increased from acceptor to donor groups. Chloro unit is the weakest acceptor, there appears a separation beginning with the chlorine (Figure 3.17).

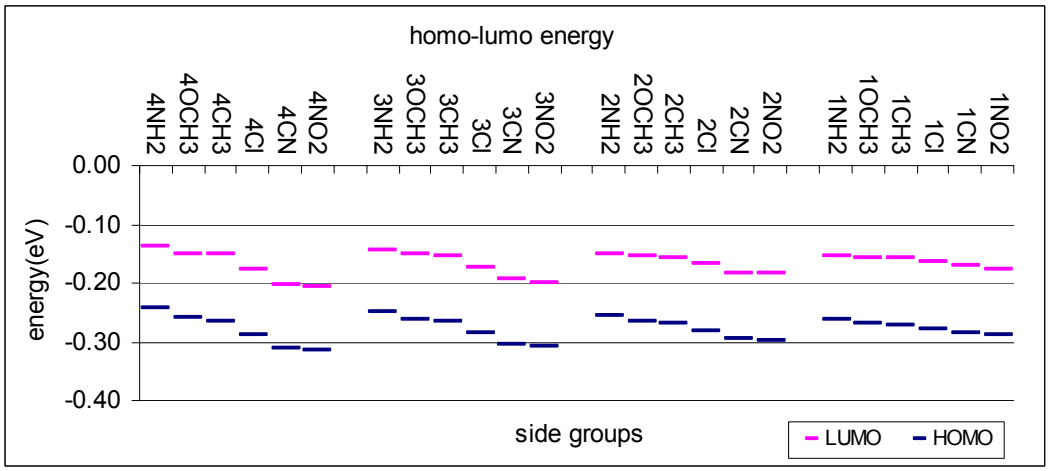

Figure 3.17. HOMO-LUMO energy levels of 1R, 2R, 3R, 4R

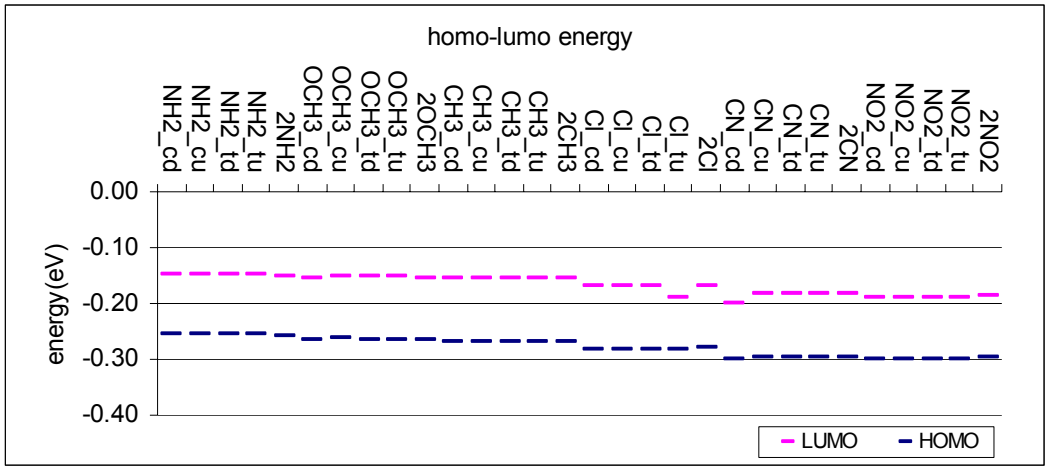

Figure 3.18. HOMO-LUMO energy levels of 2R isomers

Adding 2R groups to different rings did not affect the HOMO-LUMO energies and gap. The same trend was seen, both HOMO and LUMO energies increased from acceptor to donor groups (Figure 3.18).

When one D/A unit is bonded to benzimidazole ring the most strongest D/A increases λ_{max} about 15-20 nm with respect to moderate ones whereas adding two units on the same ring, λ_{max} increased for NH_2, decreased for NO_2 and moderates are not affected. Addition one of them on the next ring increased the wavelength of NO_2 (Figure 3.19).

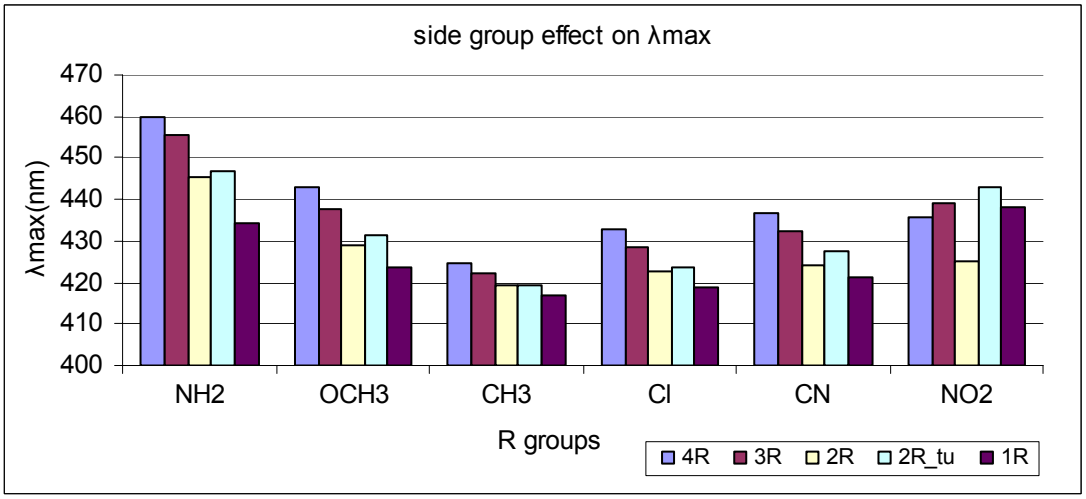

Figure 3.19. λ_{max} of the 1R, 2R, 3R, 4R

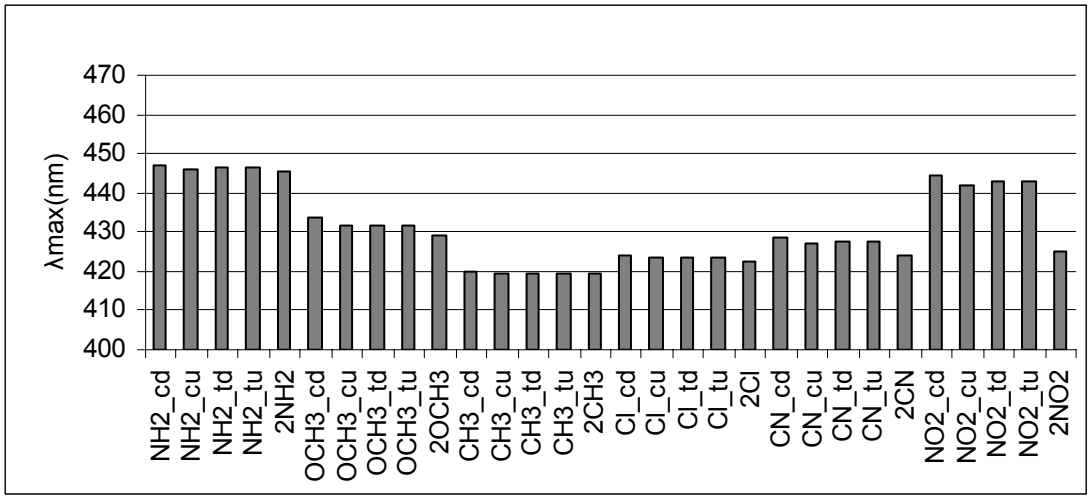

Figure 3.20. λ_{max} of the 2R isomers

When 2R groups attached to the different region on the benzimidazole ring, λ_{max} values are almost the same except NO_2. On the other hand, if NO_2 groups were bonded to the same side then λ_{max} decreased (Figure 3.20).

Table 3.9. The excited state compositions, oscillator strengths and λ_{max} of 4R

R-groups	Exc.State	Transition Character	Transition Probability	Oscillator Strength	λ_{max}(nm)
$4NH_2$	S1	H;L*	0.63	1.69	460.08
	S2	H-1;L	0.66	0.01	368.46
		H;L+1	-0.20		
$4OCH_3$	S1	H;L	0.62	1.82	442.78
	S2	H-1;L	0.64	0.00	337.09
		H;L+1	-0.25		
$4CH_3$	S1	H;L	0.62	1.83	424.40
	S2	H-1;L	0.58	0.00	306.65
		H;L+1	0.40		
4Cl	S1	H;L	0.62	1.89	432.84
	S2	H-1;L	0.58	0.00	320.29
		H;L+1	0.40		
4CN	S1	H;L	0.62	2.02	436.61
	S2	H-2;L	-0.12	0.01	346.26
		H;L+2	0.68		
$4NO_2$	S1	H;L	0.62	1.86	435.96
	S2	H;L+1	0.68	0.03	408.39
		H;L+2	-0.10		

*H and L refer to HOMO and LUMO, oscillator strengths are in arbitrary units.

The transition character with their transition probabilities, oscillator strengths and λ_{max} values are given in Table 3.9 for the first two excited states. For all substituents the main contributions to the first excited state are coming from H→L. The second excited state transition is formed by H-1→L and H→L+1 for donors including Cl but the weighted one is H-1→L. For acceptors H-2→L, H→L+1 and H→L+2 are the most participitated orbitals. For CN, H→L+2 and for NO_2, H→L+1 are the dominant ones.

4R	HOMO	LUMO
NH_2	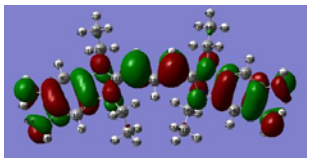	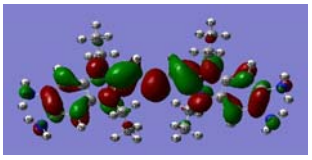
OCH_3	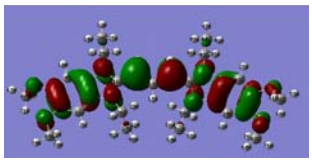	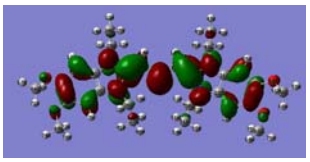
CH_3	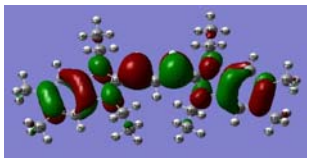	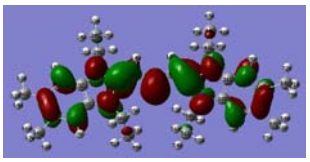
Cl	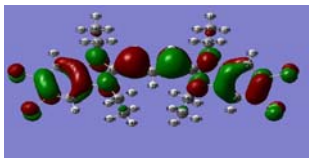	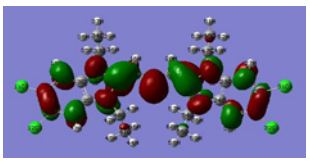
CN	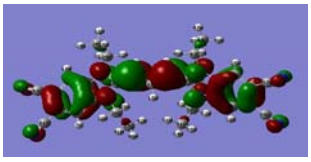	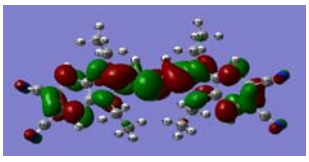
NO_2	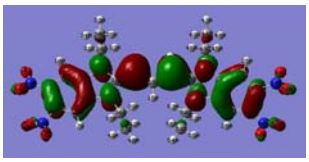	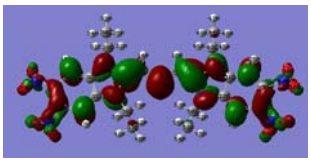

Figure 3.21. HOMO-LUMO figures of 4R

All transitions to the first excited state have HOMO to LUMO character with large oscillator strength. The intensities of the second transitions are very small. A nice

electron conjugation is seen in HOMO-LUMO electron densities. The electron D/A properties that is electron transfer from donor to molecule or molecule to acceptor are observed in those figures as expected. However, there is no electron migration from/to CH_3 /CN units (Figure 3.21).

3.2.2. Effect of Polymethine Chain Length

In this section, the chain length of polymethine group effect on the ground and excited state properties were investigated. Elongation of the chain length (Figure 3.22), did not change the bond lengths and angles much, therefore the geometry of the molecule remains almost same.

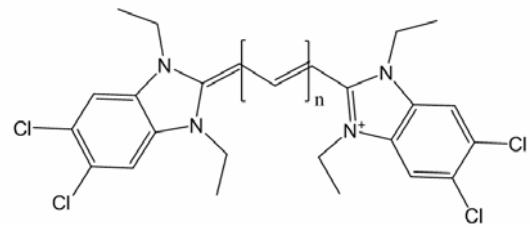

Figure 3.22. Length of the polymethine chain

Table 3.10. Dihedral angles of the polymethine chain; **n** is the number of carbon atoms

n→	3	5	7	9
D.Angle(°)	19.57	19.34	18.37	17.63

The deviation from planarity is only about 2^o from 9 Carbon to 3 Carbon atoms (Table 3.10).

The total charge of the benzimidazole groups decreased and total charge of polymethine chain increased from 3 Carbon to 9 Carbon and charge of the ethyl groups were not affected. But the total charge on benzimidazole is almost zero so the changes of the charges can be disregarded. The charge on polymethine chain becomes twice as magnitude from 3-9 carbon atoms (Table 3.11 and Figure 3.24).

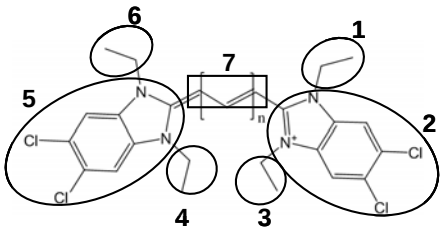

Figure 3.23. Charge groups on cyanine dye derivatives with different polymethine chain length

Table 3.11. Mulliken charges of cyanine dye derivatives with different polymethine chain length

n → / Group no	3	5	7	9
1	0.283	0.282	0.280	0.278
2	0.004	-0.001	-0.013	-0.020
3	0.268	0.271	0.271	0.272
4	0.268	0.272	0.271	0.272
5	0.004	-0.001	-0.013	-0.020
6	0.283	0.282	0.280	0.278
7	-0.110	-0.101	-0.079	-0.054

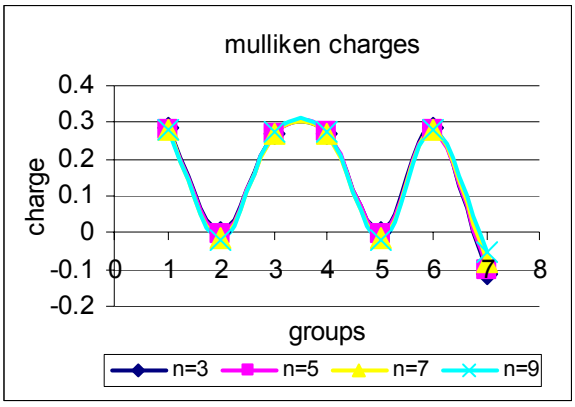

Figure 3.24. Mulliken charges of cyanine dye derivatives with different polymethine chain length

According to Table 3.12 and Figure 3.25 HOMO energies increases with the lengthening the polymethine chain while LUMO energies almost remain same. The

HOMO-LUMO gap decreases from n=3 to n=9 by the effect of HOMO energies. Therefore λ_{max} values shifted to longer wavelengths.

Table 3.12. HOMO-LUMO energies of cyanine dye derivatives with different polymethine chain length

n→	3	5	7	9
E_{LUMO} (eV)	-0.176	-0.177	-0.178	-0.177
E_{HOMO} (eV)	-0.287	-0.272	-0.260	-0.249
E_{LUMO} - E_{HOMO}	0.111	0.095	0.082	0.072

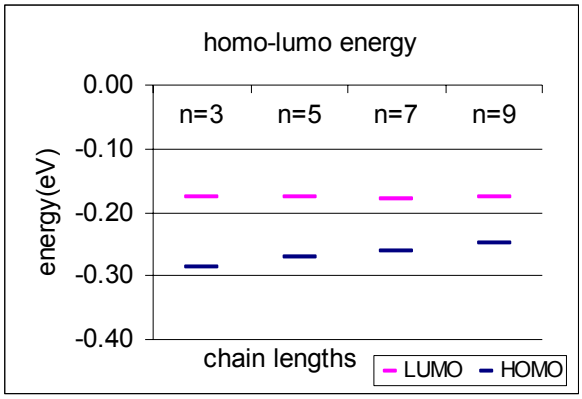

Figure 3.25. HOMO-LUMO energies of cyanine dye derivatives with different polymethine chain length

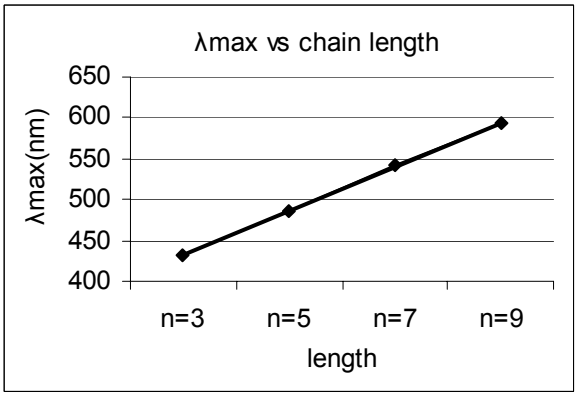

Figure 3.26. λ_{max} of cyanine dye derivatives with different polymethine chain length

The excited state calculations showed that λ_{max} values of the molecule was red shifted about 50 nm for each addition of C_2H_4 group (Figure 3.26). Conjugation of the molecule increases and bathochromic shift is observed. The similar results also observed in experimental studies; increasing the length of the polymethine chain of the different carbocyanine dyes shifted the maximum absorption wavelengths longer about 100 nm for each addition of C_2H_4 group (Fisher and. Hamer 1936; Kachkovsky, et al. 2006).

The high oscillator strength corresponds to high intense peak. It was increased approximately 0.5 arbitrary units with elongation of the chain. The transition nature of S_0 to S_1 is mainly HOMO to LUMO. The second and all higher transitions have almost zero oscillator strengths (Table 3.13).

Table 3.13. The excited states compositions, oscillator strengths and λ_{max} of cyanine dye derivatives with different polymethine chain length

n	Exc.State	Transition Character	Transition Probability	Oscillator Strength	λ_{max} (nm)
3	S1	H;L	0.62	1.89	432.84
	S2	H-1;L	0.58	0.00	320.29
		H;L+1	0.40		
5	S1	H;L	0.60	2.47	486.86
	S2	H-1;L	0.54	0.00	348.19
		H;L+1	-0.45		
7	S1	H;L	0.58	3.01	541.31
	S2	H-1;L	0.52	0.00	381.37
		H;L+1	0.47		
9	S1	H-1;L+2	0.11	3.51	594.3
		H;L	0.57		
	S2	H-1;L+1	0.51	0.00	419.91
		H;L+2	-0.48		

The electrons spread out on the backbone of the molecule. There is no electron density on ethyl groups which are perpendicular to molecular plane. The donor ability of the Cl atoms decrease as a result of elongation of the chain length. The electron density on Cl atoms gradually disappear from n=3 to n=9 in HOMO pictures (Figure 3.27). The π, π^* nature of HOMO-LUMO were not effected by the lengthening.

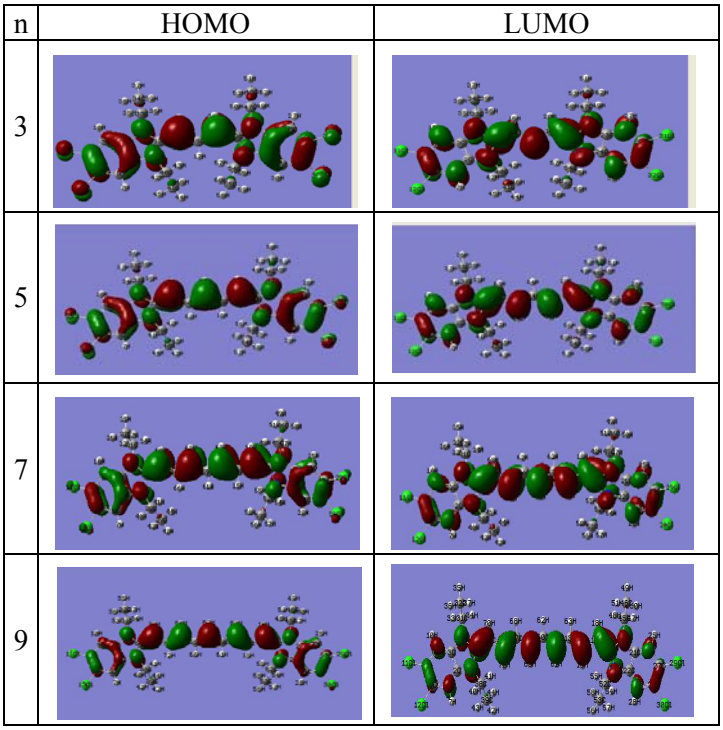

Figure 3.27. HOMO-LUMO of cyanine dye derivatives with different polymethine chain length

3.2.3. Effect of Length of Alkyl Groups

In this part, the effect of the size of the alkyl groups attached to nitrogen atoms was investigated. The X groups in Figure 3.28 were changed as Hydrogen, Methyl, Ethyl, Propyl and Butyl groups.

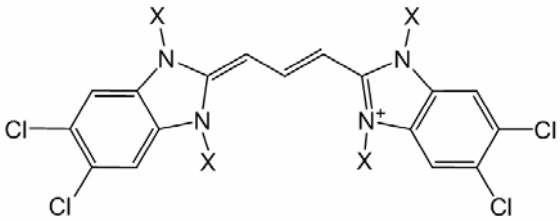

Figure 3.28. Cyanine dye derivatives with different alkyl groups

Although there is no considerable change on the bond lengths and angles by the alkyl size, the dihedral angle between benzimidazole ring and polymethine chain is changed; Hydrogen, Propyl, Butyl containing molecules are planar but Methyl and Ethyl substituted ones have torsional angle of about 20^{o} (Figure 3.29).

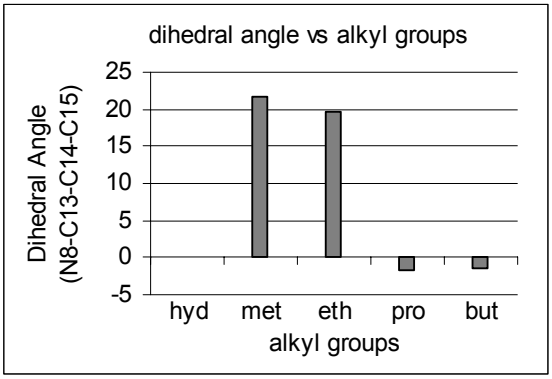

Figure 3.29. Dihedral angles of cyanine dye derivatives with different alkyl groups

Almost all the positive charges are on the alkyl groups for all derivatives, each alkyl has around +0.3 charge. The benzimidazole rings have around zero charges whereas the polymethine chain negatively charged. If deviation from planarity is observed then the charge on the benzimidazole changed from negative to positive and the charge on the chain becomes more negative (Table 3.14).

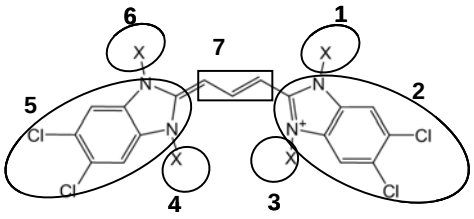

Figure 3.30. Charge groups on cyanine dye derivatives with different alkyl groups

Table 3.14. Mulliken charges of cyanine dye derivatives with different alkyl groups

X→ Group no	hyd	met	eth	pro	but
1	0.300	0.278	0.283	0.296	0.299
2	-0.062	0.011	0.004	-0.026	-0.031
3	0.289	0.261	0.268	0.282	0.285
4	0.289	0.261	0.268	0.282	0.285
5	-0.062	0.011	0.004	-0.026	-0.031
6	0.300	0.278	0.283	0.296	0.299
7	-0.052	-0.106	-0.110	-0.105	-0.104

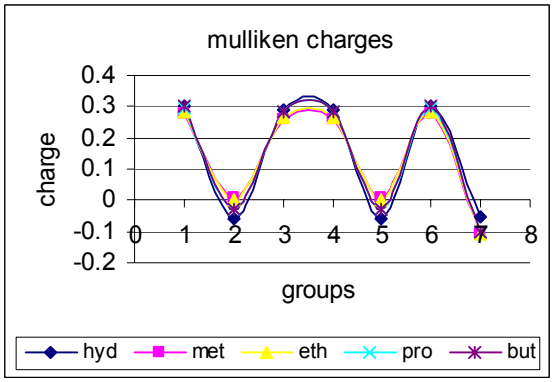

Figure 3.31. Mulliken charges of cyanine dye derivatives with different alkyl groups

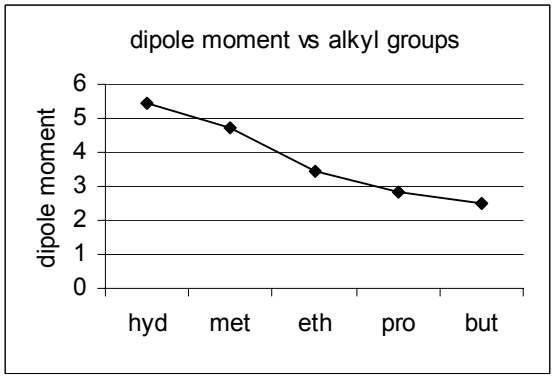

Figure 3.32. Dipole moments of cyanine dye derivatives with different alkyl groups

The dipole moments of the dye molecules displayed in Figure 3.32 decreased from Hydrogen to Butyl group. If we compare dipoles of the derivatives with consecutive alkyl size, the largest difference is observed in dipoles between Methyl and

Ethyl substituted derivatives. The dyes with Propyl and Butyl groups have almost similar dipoles. The change in dipoles is only three debye from Hydrogen to Butyl.

Both E_{LUMO} and E_{HOMO} were slightly increased up to ethyl then remain same. HOMO-LUMO gap did not change much (Figure 3.33 and Table 3.15).

Table 3.15. HOMO-LUMO energies of cyanine dye derivatives with different alkyl groups

X→	hyd	met	eth	pro	but
E_{Lumo} (eV)	-0.191	-0.179	-0.176	-0.176	-0.174
E_{Homo} (eV)	-0.302	-0.292	-0.287	-0.284	-0.282
E_{Lumo} - E_{Homo}	0.111	0.113	0.111	0.108	0.108

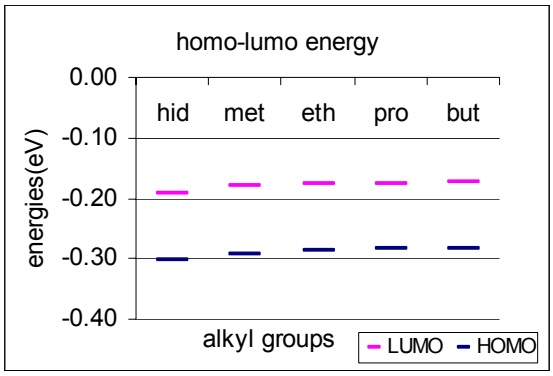

Figure 3.33. HOMO-LUMO energies of cyanine dye derivatives with different alkyl groups

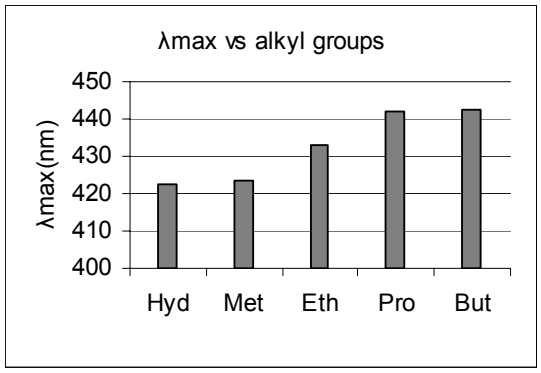

Figure 3.34. λ_{max} of cyanine dye derivatives with different alkyl groups

Hydrogen and Methyl substituted ones have λ_{max} values around 420 nm in Figure 3.34. The λ_{max} increased 10 nm for Ethyl and another 10 nm increase is observed for Propyl and Butyl with same wavelength ($\lambda_{but}=\lambda_{pro}>\lambda_{eth}>\lambda_{met}=\lambda_{hyd}$).

Table 3.16. The excited states compositions, oscillator strengths and λ_{max} of cyanine dye derivatives with different alkyl groups

Alkyl Groups	Exc.State	Transition Character	Transition Probability	Oscillator Strength	λ_{max} (nm)
hyd	S1	H;L	0.61	2.00	422.30
	S2	H-1;L	0.65	0.02	324.95
		H;L+1	-0.22		
met	S1	H;L	0.62	1.90	423.75
	S2	H-1;L	0.61	0.00	319.09
		H;L+1	0.34		
eth	S1	H;L	0.62	1.89	432.84
	S2	H-1;L	0.58	0.00	320.29
		H;L+1	0.40		
pro	S1	H;L	0.62	1.87	441.99
	S2	H-1;L	0.61	0.00	321.82
		H;L+1	0.35		
but	S1	H;L	0.62	1.83	442.65
	S2	H-1;L	0.60	0.00	321.33
		H;L+1	-0.36		

The transition nature to the first excited state is again HOMO to LUMO with high oscillating strength. The higher transitions are almost forbidden (Table 3.16).

The alkyl groups did not affect the HOMO and LUMO shapes as shown in Figure 3.35.

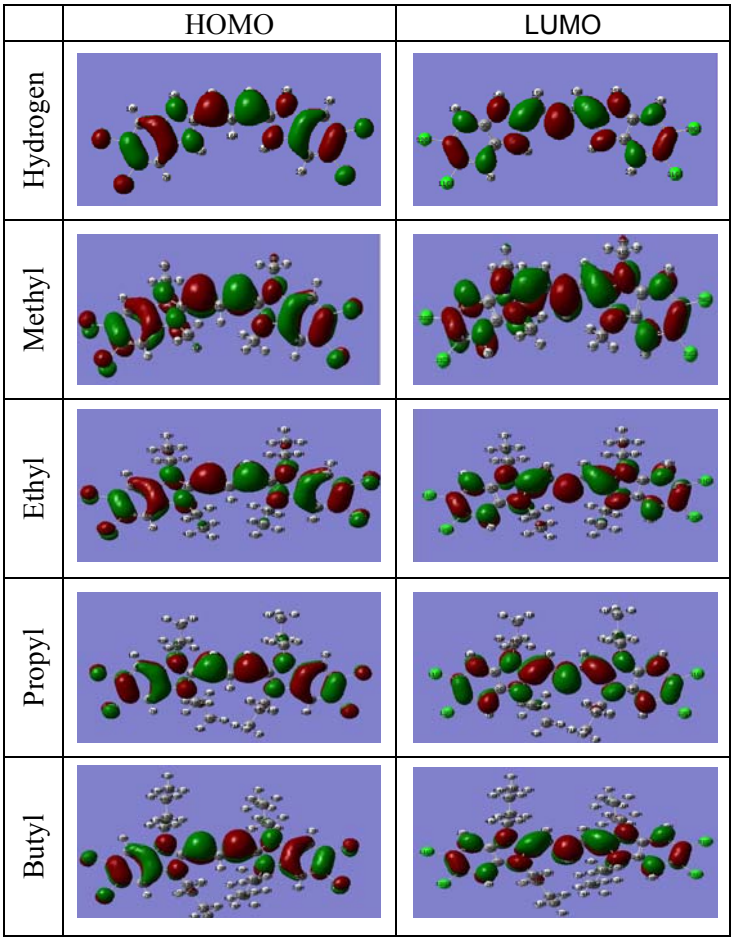

Figure 3.35. HOMO-LUMO figures of cyanine dye derivatives with different alkyl groups

3.3. Excited State Calculations

In this section excited state behaviors of TTBC were analyzed with TDDFT and CIS calculations on the ground state structures obtained by DFT with different functionals and basis sets. In addition to those solvent effects on the excited states were also investigated for TTBC molecule.

3.3.1. Potential Energy Surface (PES) Calculations of TTBC

In this part ground (S_0) and the first excited singlet state (S_1) potential energy surface sections of TTBC were obtained as a function of the twisting angles **(1)** and **(2)** as shown in Figure 3.36 to explain the shoulder on the experimental fluorescence spectrum. The question here is there a twisted intra molecular charge transfer state or not?

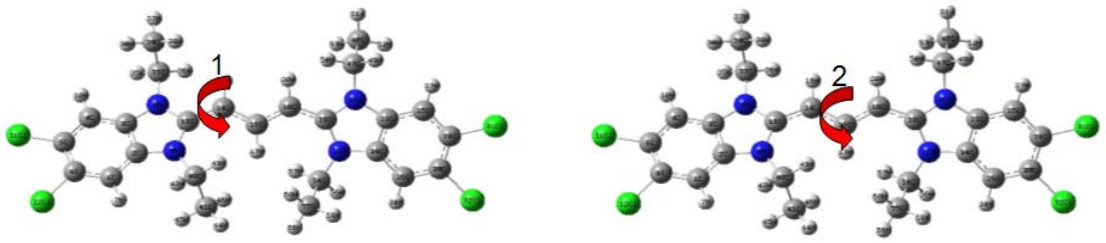

Figure 3.36 Rotation angle from two different carbon-carbon bonds of the TTBC

Geometry optimization and frequency calculations of the TTBC were performed at DFT/B3LYP/6-31G(d,p) level of theory. Excited State calculations were done both with TDDFT/B3LYP/6-31G(d,p) and CIS/6-31G(d,p). Single excitations were considered only. The molecule was rotated from different parts of the polymethine chain as explained above by the increment of 15^o from the ground state structure between -180^o and $+180^o$. Both relaxed and frozen potential energy surface (PES) sections are obtained. In the relaxed calculations all geometrical parameters except the given dihedral angle are optimized. In the frozen calculations there is no optimization. All the energies are given relative to ground state minimum structure. The excited state energies were obtained by adding vertical excitation energies to the corresponding ground state energies. The vertical excitation is the transition from the ground state to the excited state with exactly the same geometry.

In this thesis TD1 and TD2 notations refer to TDDFT calculation with rotation angle of (**1**) and (**2**) respectively**.** CIS1 and CIS2 refers to CIS calculation with rotation angle of (**1**) and (**2**) respectively.

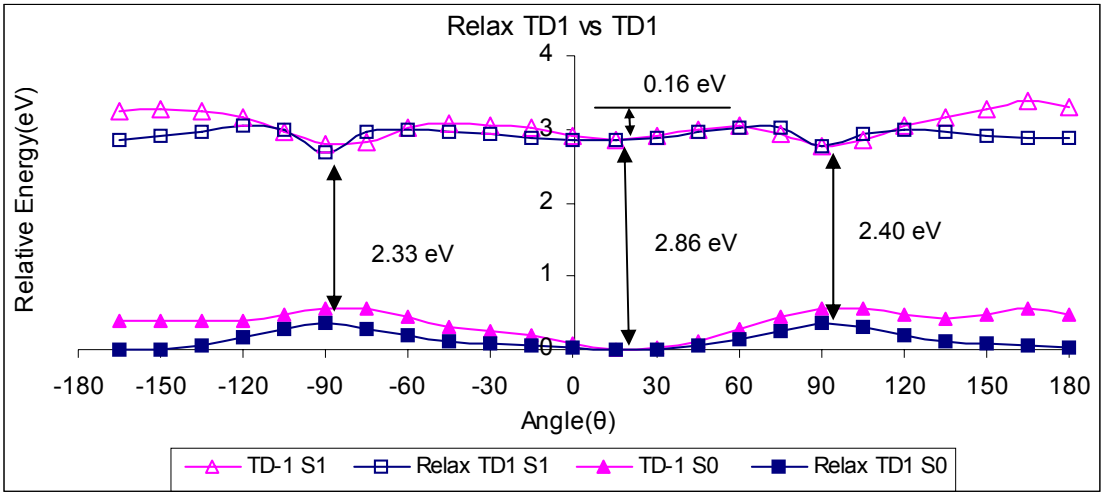

Figure 3.37. Potential energy surface section with reaction coordinate (1) of TTBC

In Figure 3.37 the PES section with reaction coordinate **(1)** is given both for relaxed and frozen calculations. The ground state energies decrease in relaxed mode as expected. But the excited state energies are almost same in both calculations. There is no optimization effect on excited state energies. A minimum point is detected in the excited state surface with the barrier height of 0.16 eV at the twisted geometry and there is a maximum at the same point in the ground state. The excitation energies from the ground state minimum structure and perpendicular structures (90^o/-90^o) are 2.86 eV (434 nm) and 2.40/2.33 eV (517/532 nm) respectively. According to Figure 3.37 there are two emission sources. These theoretical results assign that the molecule have dual emission.

From now on all the figures are given for calculations in relax mode.

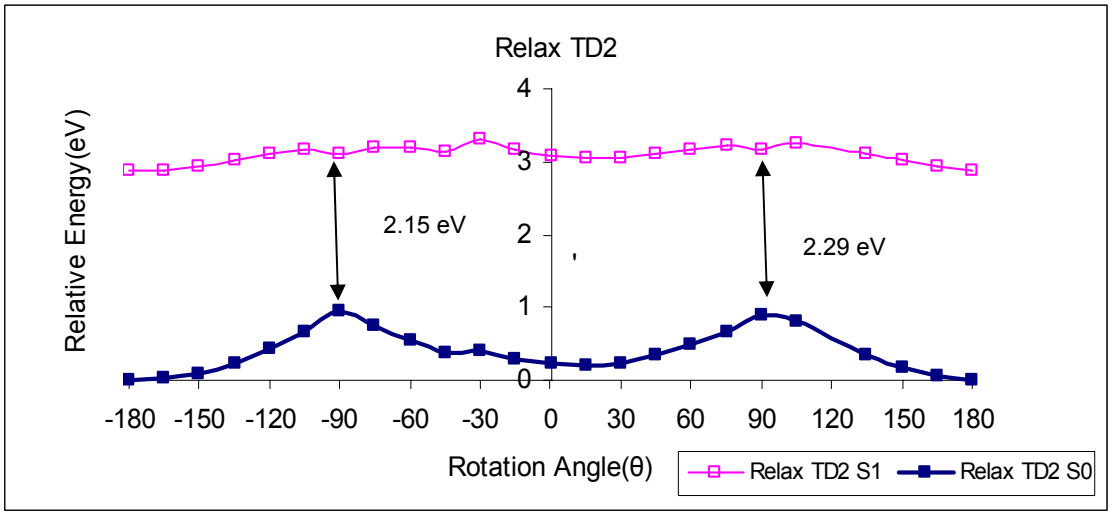

Figure 3.38. Potential energy surface section with reaction coordinate **(2)** of TTBC

For the second rotation coordinate (2) there is no minimum at the perpendicular configuration, there is almost a flat surface in the excited state (Figure 3.38).

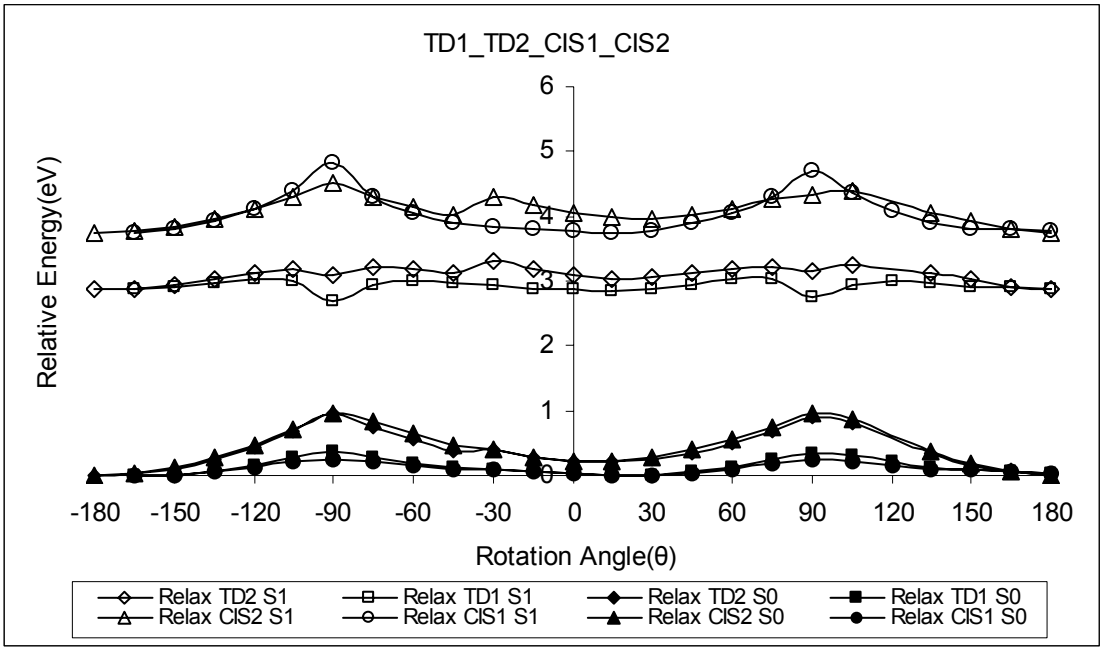

Figure 3.39. PES section with reaction coordinate **(1)** and **(2)** for both TDDFT and CIS methods

The TDDFT/B3LYP/6-31G** and CIS/6-31G** methods were used to find out the potential energy surface of the molecule in both relaxed and frozen mode. PESs explored from both CIS and TDDFT method for coordinate **(1)** and **(2)** are all collected in Figure 3.39. The ground state energies of the dye are almost the same in both methods. But the excited state behavior of the dye is different particularly at the 90^{o}. The calculated relative energy of the CIS one gave a maximum, on the otherhand the TDDFT has a minimum energy value. The excited state energies obtained from CIS are much higher than TDDFT. The λ_{max} values for CIS are far away from the experimental results. According to our calculations CIS methods is not reliable for the spectroscopic calculations of cyanine dyes.

The rotational calculations of TTBC have been performed with different functionals in gas phase and in methanol. B3LYP and PBEPBE functionals were used with 6-31G** basis set. In solvent calculations IEFPCM is used. Figure 3.40a, Figure 3.41a, and Figure 3.42a contain PES sections for ground and three lowest lying excited states with B3LYP in gas phase, B3LYP in methanol and PBEPBE functional in gas

phase respectively. They show that, the ground state energy profiles have similar trends in all methods. The solvent did not change the ground state minimum structure. With both functionals there is a minimum at the twisted configuration in the first excited state but it disappears in solvent. The second and third excited states are close to each other but far from the first one, in PBEPBE at twisted geometry they become degenerate. Figure 3.40b, Figure 3.41b, and Figure 3.42b include the energy profiles of six frontier orbitals (three virtual and three occupied) as a function of rotation angle (1) with B3LYP in gas phase, B3LYP in methanol and PBEPBE functional in gas phase respectively.. Again all the methods have similar property, the degeneracy in HOMO-2 and HOMO-1 are not disturbed by rotation. The highest two LUMO orbitals are close to each other. The solvent shifts up all the energies and HOMO-LUMO gap is smaller in PBEPBE.

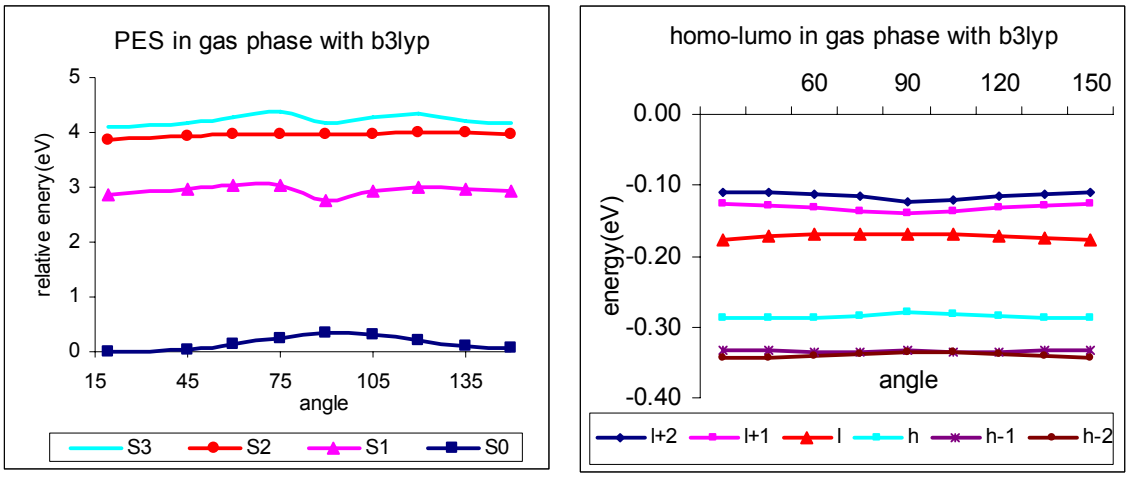

(a) (b)

Figure 3.40. (a) PES sections for ground and three lowest lying excited states (b) MO energies of six frontier orbitals (three virtual and three occupied) as a function of rotation angle **(1)** with B3LYP in gas phase

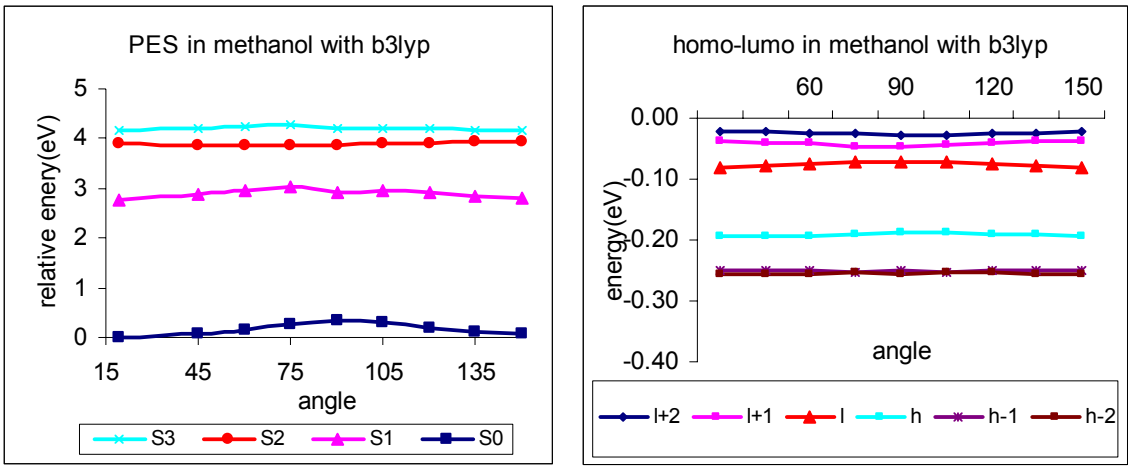

(a) (b)

Figure 3.41. (a) PES sections for ground and three lowest lying excited states (b) MO energies of six frontier orbitals (three virtual and three occupied) as a function of rotation angle **(1)** with IEFPCM/B3LYP in methanol.

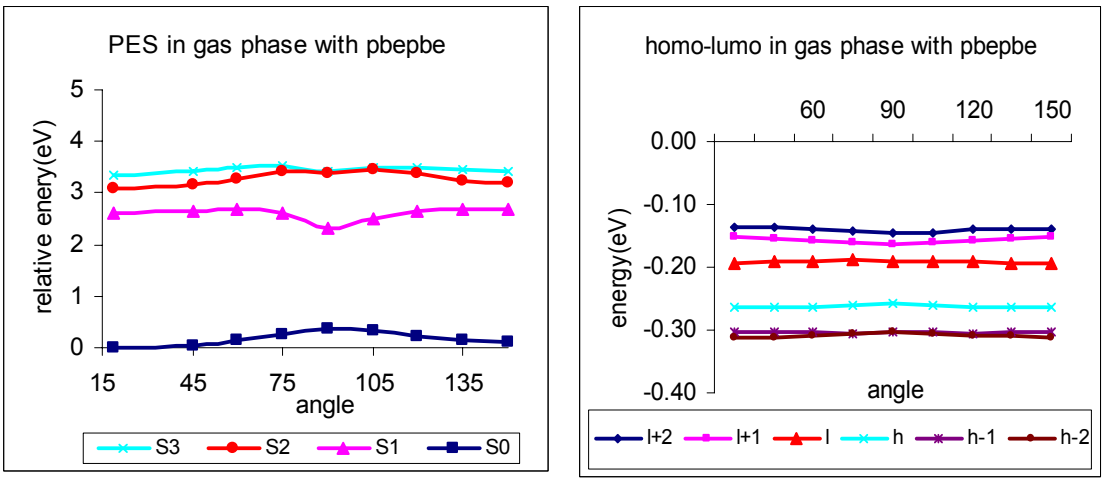

(a) (b)

Figure 3.42. (a) PES sections for ground and three lowest lying excited states (b) MO energies of six frontier orbitals (three virtual and three occupied) as a function of rotation angle **(1)**with PBEPBE in gas phase

Although the magnitude of energies and wavelengths are different, any of two functionals could be chosen since they show the similar trend.

According to Lippert equation (3.1) (Lakowicz 1999), intermolecular reorganization energy, λ_{IN} ; the orientational polarizability, Δf $(((\epsilon-1)/(2\epsilon+1))-((n^2-1)/(2n^2+1))$, where ϵ is the dielectric constant and n is the refractive index of the solvent); the difference of the dipole moments of the excited and ground state (μ_E-μ_G) ; and characteristic dimension, a. The Stokes shift must increase with the orientational polarizability. But in the experimental results the Stokes shift is about 510 cm^{-1} and does not change with the orientational polarizability. It means that the magnitude of the dipole moments in the excited state must be similar in the ground state. So, the second term of the equation can be disregarded then the Stokes shift proportional the intramoleculer reorganization energy (Ozcelik 2002).

$$\Delta\bar{\nu} \equiv \bar{\nu}_{abs} - \bar{\nu}_{emis} = 2\frac{\lambda_{IN}}{hc} + \frac{(\vec{\mu}_E - \vec{\mu}_G)^2}{2\pi\varepsilon_0 hca^3}\Delta f \qquad (3.1)$$

In this study the dipole moments of the ground and the excited states were calculated. At first the molecule twisted as in the Figure 3.43 and Figure 3.44 afterwards the ground state (μ_G) and excited state (μ_E) dipole moments were determined by the CIS/6-31G** method.

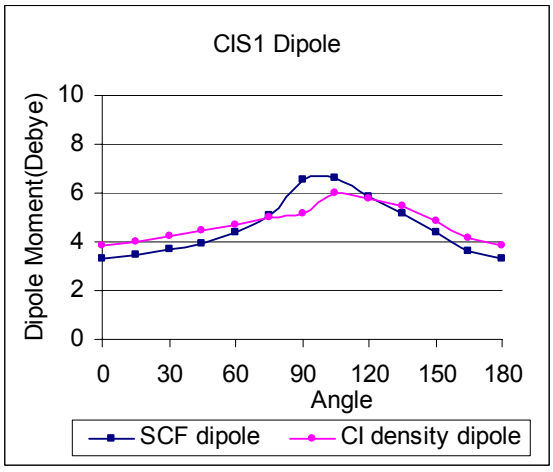

Figure 3.43. SCF ground state dipole and CI density dipole of TTBC

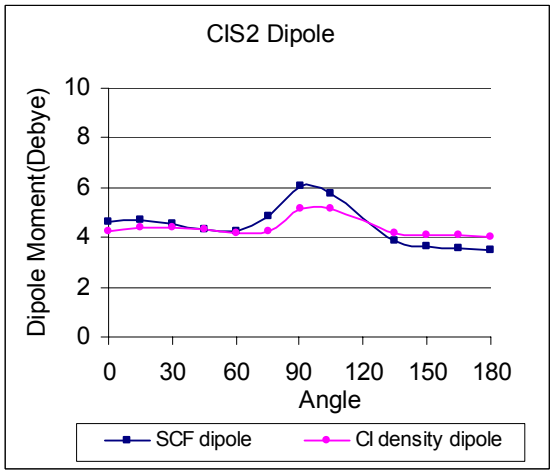

Figure 3.44. SCF ground state dipole and CI density dipole of TTBC

The difference between the excited state and ground state dipoles were positive and negative values. If it is positive it means that the excited state of the molecule is more polar than the ground state structure. The ground and excited state dipole moments are almost the same so the agreement between theory and experiment is pretty good. The polarity of the molecule depends on its electron distribution. At the 90th degrees the molecule has a charge transfer from one side to other side (Figure 3.45 and Figure 3.46). So the dipole moment values are higher nearly at 90th degrees.

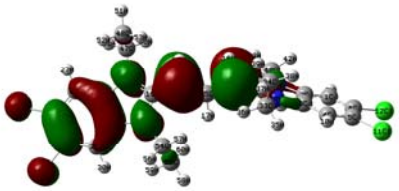

Figure 3.45. HOMO of the TTBC at 90^{o}

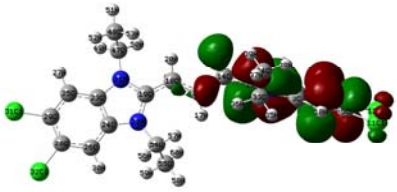

Figure 3.46. LUMO of the TTBC at 90^{o}

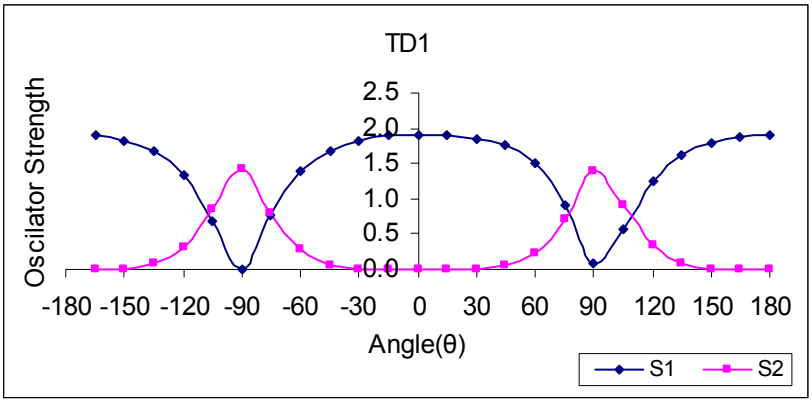

Figure 3.47. Oscillator strength of S1 and S2 state with TD**(1)**

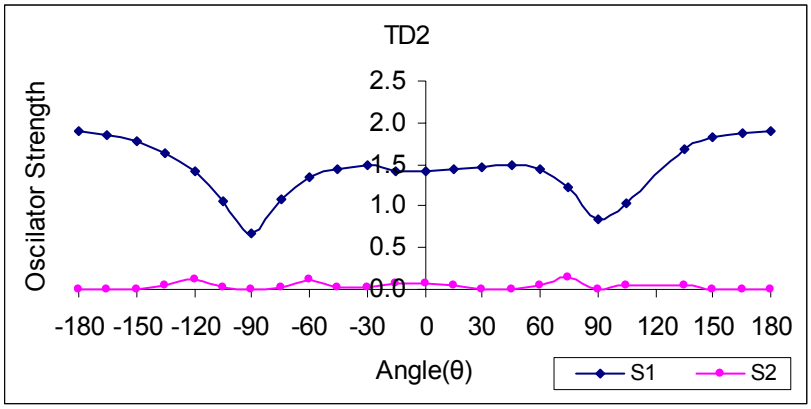

Figure 3.48. Oscillator strength of S1 and S2 state with TD**(2)**

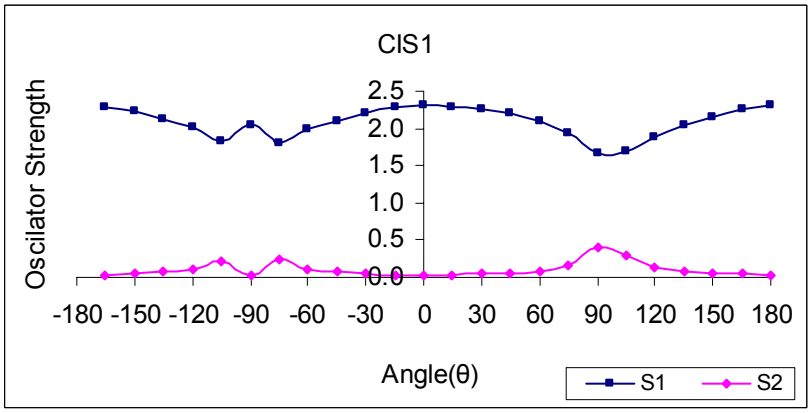

Figure 3.49. Oscillator strength of S1 and S2 state with CIS**(1)**

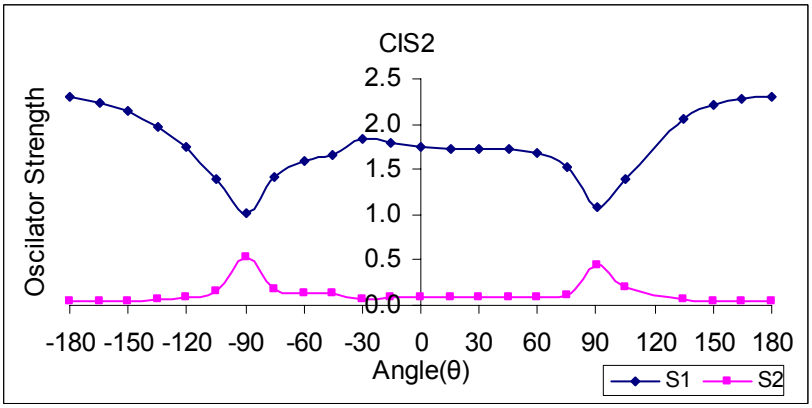

Figure 3.50. Oscillator strength of S1 and S2 state with CIS**(2)**

The oscillator strengths are demonstrated in Figure 3.47, Figure 3.48, Figure 3.49, and Figure 3.50, for TDDFT and CIS methods and reaction coordinates (**1)**, (**2)**. In all cases, the first excited state has a minimum at twisted configuration but it becomes zero only in TD(1). However the second excited state oscillates around zero but it gives a sharp maximum for TD(1).

The summary of this section can be given as, all the above results reveals that, there is no TICT state which explain the shoulder of the experimental spectrum. Although the twisted structure is favorable in the excited state with zero oscillator strength, the dipoles did not change much and there is no solvent effect in the spectrum.

3.3.2. The Basis Sets and DFT Functionals Effects on the Excited State of TTBC

In this part of the study, the basis sets and DFT functionals effects on the excited state of TTBC were investigated. The polarized basis sets, diffuse functions and several DFT functionals have been used at the excited state calculations to propose the optimal computational level. After that the computational results were compared with the experimental data. This part of the study was done very recently due to the computational expense. After new computer facilities are found then we have decided to perform this part.

At first the basis set with diffuse functions effect on TTBC was investigated. TD calculations with different basis sets were performed on the ground state structure obtained by B3LYP/6-31G(d,p). The diffuse functions and split valence effects are shown in Table 3.17 and Figure 3.51.

Table 3.17. Diffuse functions effect on λ_{max}

diffuse functions	λ_{max} (nm)	osc.(f)
b3lyp/6-31g(d,p)	432.84	1.8928
b3lyp/6-31+g(d,p)	439.42	1.8670
b3lyp/6-31++g(d,p)	439.56	1.8644
b3lyp/6-311g(d,p)	437.80	1.8857
b3lyp/6-311+g(d,p)	441.25	1.8641
b3lyp/6-311++g(d,p)	441.33	1.8626

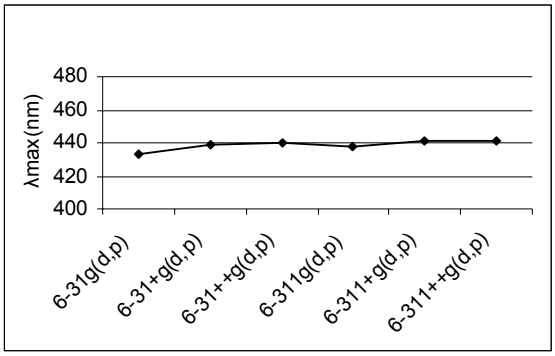

Figure 3.51. Diffuse functions effect on λ_{max}

When we add diffusion functions on heavy atom, the λ_{max} increased by 6 nm but adding diffusion functions on hydrogen atom has no effect. λ_{max} went up by 5 nm with triple split valance basis set (6-311) compared to double split (6-31) when there is no diffusion function. However there is only 2 nm difference when there is a diffuse functions. Both diffusions and split valance affect red shifted λ_{max} by 8 nm.

Then the basis set with polarization effect on TTBC was examined. The results are summarized in Table 3.18 and Figure 3.52.

Table 3.18. Polarization effect on λ_{max}

polarization functions	λ_{max} (nm)	osc.(f)
b3lyp/6-31g	427.68	1.9286
b3lyp/6-31g(d)	432.14	1.9015
b3lyp/6-31g(d,p)	432.84	1.8928
b3lyp/6-31g(2d,2p)	435.34	1.8973
b3lyp/6-31g(df,pd)	432.99	1.8881
b3lyp/6-31g(2df,2pd)	435.03	1.8900
b3lyp/6-31g(3d,3p)	438.58	1.8801

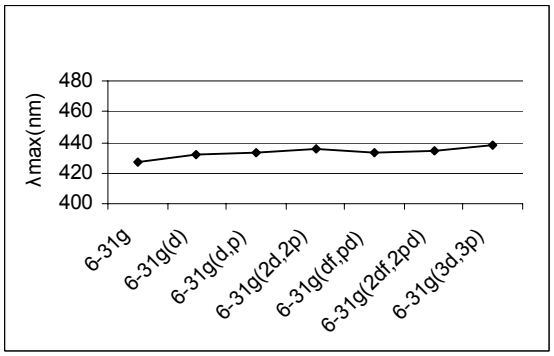

Figure 3.52. Polarization effect on λ_{max}

Addition of the polarization on heavy atom lengthening λ_{max} 4 nm but there is no effect of the polarization on hydrogen atoms. It was observed that the largest change is around 10 nm when the basis set extended with higher order polarizations (2d,2p; df,pd; 2df,2pd; 3d,dp). However the computational cost is expensed from couple of hours to 10 days for both diffusion and polarization extensions. The b3lyp/6-31g(d,p) was selected by considering the computational time.

After the selection of the basis set, the DFT functional effect was studied by changing exchange and hybrid functionals excited state computations. According to Table 3.19 and Figure 3.53, the change of the functionals was significantly effected the λ_{max} more than the diffusion and polarization extensions, but in this case computational time is almost the same. The highest wavelength (470 nm) is obtained by pbepbe functional. It is about 40 nm far from b3lyp. Lastly, the functionals are changed for both ground and excited state computations. Table 3.20 shows the λ_{max} values calculated with functionals in ground state structure optimization and excited states. When the pbepbe was used in both ground and excited state, λ_{max} was the 477 nm. Extension of the basis set with diffuse functions in ground state optimization has almost no effect but in excited state with pbepbe functional longer λ_{max} about 8 nm.

Table 3.19. Functional effect on λ_{max}

functionals*	λ_{max} (nm)	osc.(f)
mpw1pw91	424.07	1.9336
pbe1pbe	424.10	1.9346
b3pw91	431.53	1.9053
b3lyp	432.84	1.8928
hcth	466.36	1.7441
pbepbe	469.90	1.7379

*6-31g(d,p) was used in all functionals

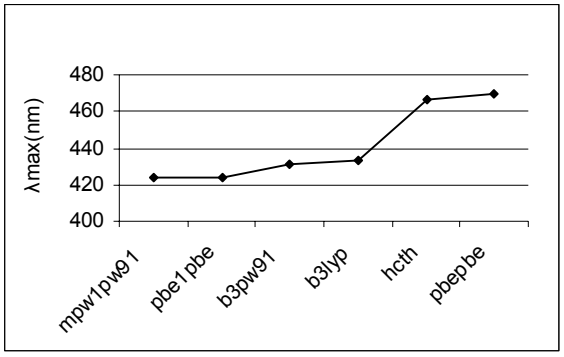

Figure 3.53. Functional effect on λ_{max}

Table 3.20. Functional effect of optimization and excited state on λ_{max}

optimization-functionals	excited-functionals	λ_{max} (nm)	osc.(f)
b3lyp/6-31g(d,p)	b3lyp/6-31g(d,p)	432.84	1.8928
pbe1pbe/6-31g(d,p)	b3lyp/6-31g(d,p)	429.71	1.8840
pbepbe/6-31g(d,p)	b3lyp/6-31g(d,p)	440.05	1.8862
b3lyp/6-31g(d,p)	pbepbe/6-31g(d,p)	469.90	1.7379
pbepbe/6-31g(d,p)	pbepbe/6-31g(d,p)	477.30	1.7320
pbepbe/6-31+g(d,p)	pbepbe/6-31g(d,p)	478.03	1.7330
pbepbe/6-31g(d,p)	pbepbe/6-31+g(d,p)	485.45	1.7044
pbepbe/6-31+g(d,p)	pbepbe/6-31+g(d,p)	486.26	1.7042

In summary, the choose of functionals are much more important in excited state than ground state. The wavelengths obtained from PBEPBE are more close to the experimental values. Finally, the experimental λ_{max} value was simulated best with the use of PBEPBE/6-31G+(d,p) for the optimization and PBEPBE/6-31+G(d,p) for the excited state calculations in gas phase.

3.3.3. CPCM and IEFPCM calculations of TTBC in different solvents

In the last part, the solvent effect on the λ_{max} value was analyzed with Conductor-like Polarizable Continuum Model (CPCM) and Integral Equation Formalism Polarizable Continuum Model (IEFPCM) solvation models. Seven solvents are used with dielectric constant ranging from 9 to 78. The level of calculations are shown in Table 3.21 for ground state and excited states. The λ_{max}s computed with different level of calculations are listed in Table 3.22. Up to now, it was observed that the functional pbepbe and diffusion extension of basis set red shift the λ_{max} by almost 50 nm with respect to b3lyp/6-31g** in the gas phase. The addition of solvent extends the wavelength by 15-20 nm for both functionals. These findings are summarized in Figure 3.54. This figure also covers the experimental results with four solvents which are common in our calculations (Table 3.23). It is seen that, the absorption of the λ_{max} values did not change much with the dielectric constants at different levels of theory. This indicates that the λ_{max} is independent of the polarity of the solvent. These results are consistent with the experimental conclusions. The calculations carried out with pbepbe/6-31+g** in solvent are fairly good agreement with the experiments. The error is approximately 10nm.

Table 3.21. Level of theory used in solvent calculation

	IEFPCM[1]	IEFPCM[2]*	CPCM[a]	IEFPCM[3]	CPCM[aa]
Ground State	B3LYP/ 6-31G**	B3LYP/ 6-31G**	B3LYP/ 6-31G**	PBEPBE/ 6-31+G**	PBEPBE/ 6-31+G**
Excited State	B3LYP/ 6-31G**	B3LYP/ 6-31G**	B3LYP/ 6-31G**	PBEPBE/ 6-31+G**	PBEPBE/ 6-31+G**

*Ground state geometries are in gas phase only with IEFPCM[2] the geometry was optimized in the solvent.

Table 3.22. Excited state calculation of TTBC in different solvents with CPCM&IEFPCM

Dielc. Cons.	Solvent	IEFPCM[1]	IEFPCM[2]	CPCM[a]	IEFPCM[3]	CPCM[aa]
		λ_{max} (nm)	λ_{max}(nm)	λ_{max}(nm)	λ_{max}(nm)	λ_{max}(nm)
8.9	Dichloro methane	451	452	454	506	509
20.7	Acetone	448	449	451	502	506
24.6	Ethanol	448	450	451	503	506
32.6	Methanol	447	448	450	501	504
36.6	Acetonitrile	448	449	450	502	505
46.7	DMSO	453	454	456	508	512
78.4	Water	448	-	451	503	506

Table 3.23. Experimental λ_{max} of TTBC in different solvents (Source: Ozcelik 2002)

The photophysical parameters of TTBC at room temperature

Parameters	MeOH	EtOH	PrOH	BuOH	HexOH	Ethylene glycol	Glycerol[a]	Acetonitrile	DMSO
λ_{abs} (nm)[b]	514	516	518	520	521	518	521	515	522
λ_{fluo} (nm)[c]	528	530	532	534	535	532	535	529	536
$\Delta\nu_{Stokes}$ (cm^{-1})	515	512	508	504	502	508	502	513	500

The optimizations in the solvent did not change the geometry and λ_{max} values. The CPCM and IEFPCM methods' results were very close to each other and the λ_{max} of the CPCM is larger about 3 nm than the IEFPCM method for both B3LYP and PBEPBE functions.

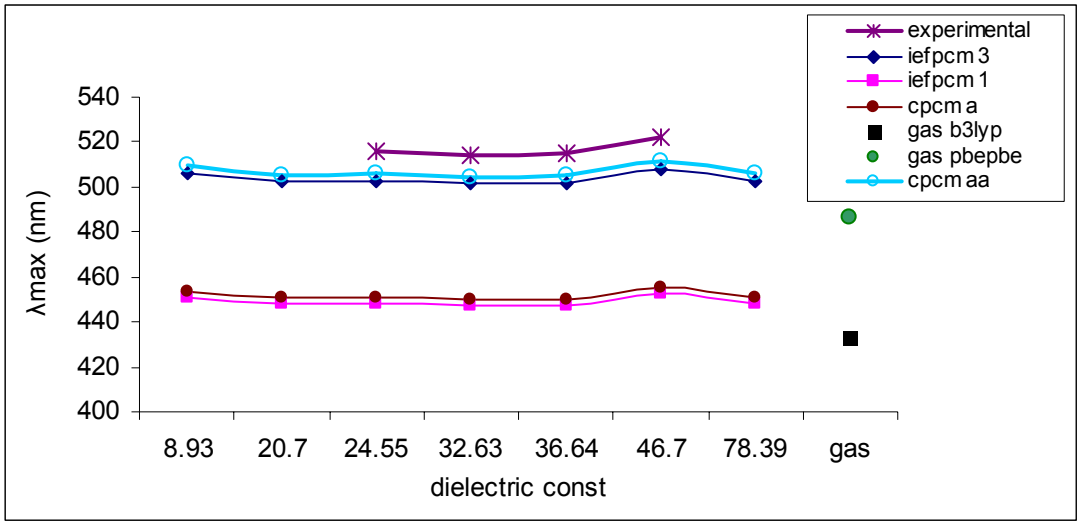

Figure 3.54. Effect of dielectric constants on λ_{max} of TTBC both experimental and computational methods

The experimental absorption spectrum and simulated spectrum with TDDFT/CPCM/PBEPBE/631+G** // DFT/PBEPBE/631+G** in different solvents are compared in (Figure 3.55and Figure 3.56).

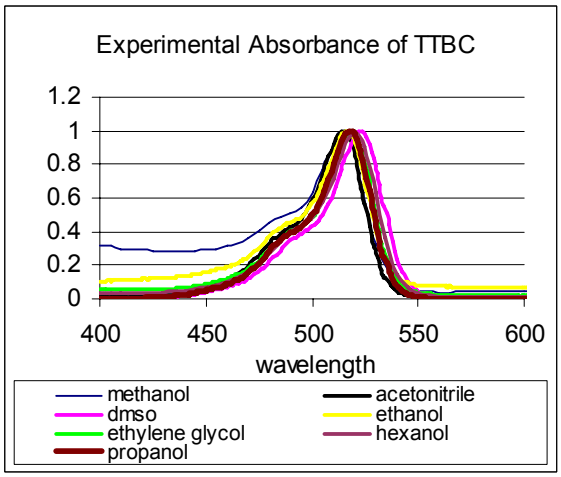

Figure 3.55. Experimental absorption spectrum

(Source: Ozcelik 2002)

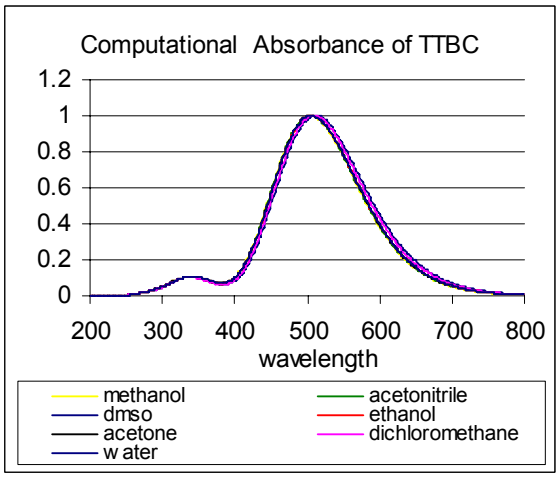

Figure 3.56. Computational absorption spectrum

* TDDFT/CPCM/PBEPBE/631+G**

Both of the experimental and computational spectra were normalized at its wavelength of maximum. They show extremely good agreement in λ_{max} value. However the shoulder which appears in the experimental spectrum did not show up in the simulated spectrum (Figure 3.55 and Figure 3.56).

CHAPTER 4

CONCLUSION

In this work, the ground state and excited state behaviors the TTBC in the gas phase and solvents were examined by using quantum chemical methods. In the ground state, the effects of functional groups on the benzimidazole rings, length of the conjugated chain, and alkyl groups bonded to the nitrogen atoms have been analyzed.

The optimum ground state has a dihedral angle of 19^o between two hetereo cyclic ring. The optimum structure is not far from X-ray structure (dihedral angle 4^o). There is no significant effect of functional groups either as donor or acceptor on the optimum structure. Only the alkyl groups attached to nitrogen atoms change the planarity of the molecule. If hydrogen, propyl and butyl groups are used instead of ethyl moieties than the molecule becomes planar. Both HOMO and LUMO energies increased from acceptor to donor groups. The donor groups especially NH_2 increases λ_{max} about 30 nm if two $N0_2$ placed in different benzimidazole rings it also tune up the λ_{max} by about 18 nm.

Increasing the conjugation length by one vinyl group increase λ_{max} by 50 nm. The HOMO energies increase linearly with chain length whereas LUMO does not change. Alkyl size may also shift λ_{max}, for butyl and propyl compared to ethyl there is 10 nm difference.

In conclusion, TTBC has a very rigid geometry. But it is possible to tune up λ_{max} with NH_2 and butyl/propyl and increasing polymethine chain length.

To explain the shoulder on the fluorescence spectrum, the PES calculations are carried out. The twisted intramolecular charge transfer character of the molecule is searched via these computations. Although in the excited state PES there exist a minimum at 90^o with zero oscillator strength but there is no sudden dipole change at twisted geometry. So TICT model does not explain the shoulder. The ground and excited state dipoles are almost same, and supported by experimental results.

The solvent effect calculations show that, λ_{max} values are independent of the polarity of the solvents as also seen experimentally.

In general, the calculations support experimental results. We hoped that with the help of this study the properties of the TTBC at the ground and excited state could be understand easily and give light into the design of the synthesis of new dye derivatives.

REFERENCES

Barone, V. and Cossi, M. 1998. Analytical second derivatives of the free energy in solution by polarizable continuum models. *The Journal of Chemical Physics* 109:6246.

Bertolino, C.A., Ferrari, A.M., Barolo, C., Viscardi, G., Caputo, G. and Coluccia, S. 2006. Solvent effect on indocyanine dyes: a computational approach. *Chemical Physics* 330:52-59.

Bowser, D.N., Minamikawa, T., Nagley, P. and Williams, D.A. 1998. Role of mitochondria in calcium regulation of spontaneously contracting cardiac muscle cells. *Biophysical Journal* 75:2004-2014.

Cancès, E., Mennucci B. and Tomasi, J. 1997.A new integral equation formalism for the polarizable continuum model: theoretical background and applications to isotropic and anisotropic dielectrics. *The Journal of Chemical Physics* 107:3032.

Casida, M.E., Gutierrez, F., Guan, J., Gadea, F.X., Salahub, D. Daudey, J.P. 2000. Charge-transfer correction for improved time-dependent local density approximation excited-state potential energy curves: Analysis within the two-level model with illustration for H_2 and LiH. *Journal of Chemical Physics* 113:7062.

Chakraborty, A., Kar, S., Nath, D.N. and Guchhait, N. 2006. Photoinduced intramolecular charge transfer reaction in (e)-3-(4-methylamino-phenyl)-acrylic acid methyl ester: a fluorescence study in combination with TDDFT calculation. *The Journal of Physical Chemistry A* 110:12089-12095.

Champagne, B., Guillaume, M. and Zutterman, F. 2006. TDDFT investigation of the optical properties of cyanine dyes. *Chemical Physics Letters* 425:105-109.

Chen, L. and Smiley, S.T. 1993. *Probing mitochondrial membrane potential in living cells by a J-aggregate-forming dye. In: Hason WT (ed) Fluorescent and luminescent probes for biological activity: a practical guide to technology for quantitative real-time analysis.* Academic Press: New York.

Cossarizza, A. and Salvioli, S. 2001. Analysis of mitochondria during cell death. *Methods Cell Biology* 63:467-86.

Cossi, M. and Barone, V. 1998. Quantum calculation of molecular energies and energy gradients in solution by a conductor solvent model. *The Journal of Physical Chemistry A* 102:1995.

Cossi, M., Rega, N,, Scalmani, G. and Barone, V. 2003. Energies, structures, and electronic properties of molecules in solution with the C-PCM solvation model. *Journal of Computational Chemistry* 24:669–681.

Cramer, J.C. 2002. *Essentials of computational chemistry: theories and models*. John. Wiley & Sons, England.

Feller, K.H., Gadonas, R. and Krasauskas, V. 1988. Picosecond absorption spectroscopy of polymethine cis-trans isomerization. *Laser Chemistry* 8:39-47.

Fisher, N.I. and Hamer, F.M. 1936. A comparison of the absorption spectra of some typical symmetrical cyanine dyes. *Proceedings of the Royal Society of London. Series A, Mathematical and Physical Sciences* 154:703-723.

Foresman, J.B. and Frisch, A., eds.1996. *Exploring chemistry with electronic structure methods: second edition*. Gaussian, Inc., USA.

Frisch, M.J., Trucks, G.W., Schlegel, H.B., Scuseria, G.E., Robb, M.A., Cheeseman, J.R., Montgomery, Jr., J.A., Vreven, T., Kudin, K.N., Burant, J.C., Millam, J.M., Iyengar, S.S., Tomasi, J., Barone, V., Mennucci, B., Cossi, M., Scalmani, G., Rega, N., Petersson, G.A., Nakatsuji, H., Hada, M., Ehara, M., Toyota, K., Fukuda, R., Hasegawa, J., Ishida, M., Nakajima, T., Honda, Y., Kitao, O., Nakai, H., Klene, M., Li, X., Knox, J.E., Hratchian, H.P., Cross, J.B., Adamo, C., Jaramillo, J., Gomperts, R., Stratmann, R.E., Yazyev, O., Austin, A.J., Cammi, R., Pomelli, C., Ochterski, J.W., Ayala, P.Y., Morokuma, K., Voth, G.A., Salvador, P., Dannenberg, J.J., Zakrzewski, V.G., Dapprich, S., Daniels, A.D., Strain, M.C., Farkas, O., Malick, D.K., Rabuck, A.D., Raghavachari, K., Foresman, J.B., Ortiz, J.V., Cui, Q., Baboul, A.G., Clifford, S., Cioslowski, J., Stefanov, B.B., Liu, G., Liashenko, A., Piskorz, P., Komaromi, I., Martin, R.L., Fox, D.J., Keith, T., Al-Laham, M.A., Peng, C.Y., Nanayakkara, A., Challacombe, M., Gill, P.M.W., Johnson, B., Chen, W., Wong, M.W., Gonzalez C., and Pople, J.A.,2003.*Gaussian 03, Revision B.05*. Gaussian, Inc., Pittsburgh PA.

Gobbi, L., Elmaci, N., Lüthi, H.P., and Diederich, F. 2001. N,N-dialkylaniline-substituted tetraethynylethenes: A new class of chromophores possessing an emitting charge-transfer state. experimental and computational studies. *ChemPhysChem* 2:101-111.

Grabowski, Z.R., Rotkiewicz K., Rettig, W. 2003. Structural changes accompanying intramolecular electron transfer: Focus on twisted intramolecular charge-transfer states and structures. *Chemical Reviews* 103:3899-4031.

Grabowski, Z.R., Rotkiewicz, K., Siemiarczuk, A. 1979. Dual fluorescence of donor-acceptor molecules and the twisted intramolecular charge transfer (TICT) states *Journal of Luminescence* 18/19:420.

Guillaumont D., Nakamura, S., 2000. Calculation of the absorption wavelength of dyes using time-dependent density-functional theory (TD-DFT). *Dyes and Pigments* 46:85-92.

Hamer, F.M. 1964. *The cyanine dyes and related compound*. New York: Interscience Publishers.

Haugland, R.P. 2006. *The handbook: a guide to fluorescent probes and labeling techniques.* Invitrogen. Carlsbad, CA. http://probes.invitrogen.com/handbook/ (accessed June 10, 2008).

Herz, A. H. 1977. Aggregation of sensitizing dyes in solution and their adsorption onto silver halides. *Advances in Colloid and Interface Science* 8:237-298.

Hirata, S. and Gordon M.H. 1999. Time-dependent density functional theory for radicals. an improved description of excited states with substantial double excitation character. *Chemical Physics Letters* 302:375.

Hirata, S., Zhan, C.G., Apr`a, E., Windus, T.L. and Dixon, D.A. 2003. A new, self-contained asymptotic correction scheme to exchange-correlation potentials for time-dependent density functional theory. *The Journal of Physical Chemistry A* 107:10154.

Hohenberg, P., Kohn, W. 1964. Inhomogeneous electron gas. *Physical Review B.* 136:864.

Huang, M., Camara, A.K.S., Stowe, D.F. and Beard, D.A. 2007. Quantitative analysis of mitochondrial membrane potential measurements with JC-1. *Federation of American Societies for Experimental Biology Journal*. 21:946.

International Union of Pure and Applied Chemistry (IUPAC), 2008. http://www.iupac.org/goldbook/C01487.pdf (accessed June 9, 2008).

Jacquemin, D., Preat, J., Wathelet, V., Fontaine, M. and Perpéte, E.A.. 2006. Thioindigo dyes: highly accurate visible spectra with TD-DFT. *Journal of American Chemical Society* 128:2072-2083.

Jelley, E. 1937. Molecular, nematic and crystalline states of 1:1'-diethylcyanine chloride. *Nature (Lond.)* 139:631-632.

Johannes, G., Stefan, B. and Dominik, M. 2006. *Computational nanoscience: do it yourself! John Von Neumann institute for computing.* Jülich: NIC Series.

Jödicke, C.J. and Lüthi, H.P. 2003. Time-dependent density functional theory (TDDFT) study of the excited charge-transfer state formation of a series of aromatic donor-acceptor systems. *Journal of American Chemical Society* 125:252-264.

Kachkovsky, A.D., Pilipchuk, N.V., Kurdyukov, V.V. and Tolmachev, A.I. 2006. Electronic properties of polymethine systems. 10. electron structure and absorption spectra of cyanine bases. *Dyes and Pigments* 70:212-219.

Kawakami, M., Koya, K., Ukai, T., Tatsuta, N., Ikegawa, A., Ogawa, K., Shishido, T., and Chen, L.B. 1998. Structure-activity of novel rhodacyanine dyes as antitumor agents. *Journal of Medicinal Chemistry* 41:130-142.

Ko, C., Malick, D.K., Braden, D.A., Friesner, R.A. and Martínez, T.J. 2008. Pseudospectral time-dependent density functional theory. *The Journal of Chemical Physics* 128:104103.

Kohn, W. and Sham, L.J. 1965. Self-consistent equations including exchange and correlation effects. *Physical. Review A.* 140:1133.

Lakowicz, J.R. 1994. *Topics in fluorescence spectroscopy vol 4: probe design and chemical sensing*. Plenum Press: New York and London.

Lakowicz, J.R. 1999. *In Principles of Fluorescence Spectroscopy, 2nd Edition*, Kluwer Academic/Plenum Publishers, New York.

Levine, I.N. 2000. *Quantum chemistry*: *Fifth Edition*. Prentice-Hall Inc.:USA.

Lippert, E., Lüder, W. and Boss, H. 1962. *Advances in Molecular Spectroscopy*. Pergamon: Oxford.

Maeda, M. 1984. *Laser dyes: properties of organic compounds for dye lasers*. Academic press: New York.

Marques, M.A.L. and Gross, E.K.U. 2004. Time-dependent density functional theory. *Annual Reviews of Physical Chemistry*. 55:427-55.

McRae, E.G and Kasha, M. 1958. Enhancement of phosphorescence ability upon aggregation of dye molecules. *The Journal of Chemical Physics* 28:721.

Mennucci, B., Cancès, E. and Tomasi, J. 1997. Evaluation of solvent effects in isotropic and anisotropic dielectrics and in ionic solutions with a unified integral equation method: theoretical bases, computational implementation, and numerical applications. *The Journal of Physical Chemistry B.* 101:10506.

Mennucci, B. and Tomasi, J. 1997. Continuum solvation models: a new approach to the problem of solute's charge distribution and cavity boundaries. *The Journal of Chemical Physics.* 106:5151.

Mishra, A., Behera, R.K., Behera, P.K., Mishra, B.K. and Behera, G.B.. 2000. Cyanines during the 1990s: a review. *Chemical Reviews* 100:1073-2011.

Nuernberger, P., Vogt, G. and Gerber, G. 2006. Femtosecond study on the isomerization dynamics of NK88. I. ground-state dynamics after photoexcitation. *The Journal of Chemical Physics* 125:044512.

Olsen, S. and Smith, S.C. 2007. Radiationless decay of red fluorescent protein chromophore models via twisted intramolecular charge-transfer states. *Journal of American Chemical Society* 129:2054-2065.

Orlandi, G. and Siebrand, W. 1975. Model for the direct photo-isomerization of stilbene. *Chemical Physics Letters* 30:352-354.

Ozcelik, S. 2002. Steady state and picosecond time-resolved photophysics of a benzimidazolocarbocyanine dye. *Journal of Luminescence* 96:141-148.

Park, J. 2000. AM1 semiempirical calculated potential energy surfaces for the isomerization of symmetrical carbocyanines. *Dyes and Pigments* 46:155-161.

Polla, B.S., Kantengwa, S., François, D., Salvioli, S., Franceschi, C., Marsac, C. and Cossarizza, A. 1996. Mitochondria are selective targets for the protective effects of heat shock against oxidative injury. *The Proceedings of the National Academy of Sciences (USA)* 93:6458-6463.

Product Spectra. 2008. Invitrogen. http://www.invitrogen.com/site/us/en/home/support/Product-Technical-Resources/Product-Spectra.3168p82.html (accessed June 10, 2008).

Reers, M., Smith, T.W. and Chens, L.B. 1991. J-aggregate formation of a carbocyanine as a quantitative fluorescent indicator of membrane potential. *Biochemistry* 30:4480-4486.

Rodriguez, J., Scherlis, D., Estrin, D., Aramendia, P.F. and Negri R.M. 1997. AM1 study of the ground and excited state potential energy surfaces of symmetric carbocyanines. *The Journal of Physical Chemistry A* 101:6998-7006.

Rulliere, C. 1976. Laser action and photoisomerisation of 3,3'-diethyl oxadicarbocyanine iodide (DODCI): Influence of temperature and concentration. *Chemical Physics Letters* 43:303-308

Runge, E. and Gross, E.K.U. 1984. Density functional theory for time-dependent systems. *Physical Review Letters* 52:997-1000.

Salvioli, S., Ardizzoni, A., Franceschi, C., Cossarizza, A. 1997. JC-1, but not DiOC6(3) or rhodamine 123, is a reliable fluorescent probe to assess delta psi changes in intact cells: implications for studies on mitochondrial functionality during apoptosis. *Federation of European Biochemical Societies Letters* 411:77-82.

Scalmania, G., Frisch, J.M., Mennucci, B. and Tomasi, J., Cami, R. And Barone, V. 2006. Geometries and properties of excited states in the gas phase and in solution: theory and application of a time-dependent density functional theory polarizable continuum model. *The Journal of Chemical Physics* 124:094107.

Sharp, A.K. and Honig, B. 1990. Electrostatic interactions in macromolecules: theory and applications. *Annual Review of Biophysics and Biophysical Chemistry*. 19:301- 332.

Siemiarczuk, A.; Grabowski, Z.R.; Krówczyński, A.; Asher, M.;Ottolenghi, M. 1977. Two emitting states of excited p-(9-anthryl)-n,n-dimethylaniline derivatives in polar solvents. *Chemical Physics Letters* 51:315.

Silva, G.L., Ediz, V., Yaron, D. and Armitage, B. A. 2007. Experimental and computational investigation of unsymmetrical cyanine dyes: understanding

torsionally responsive fluorogenic dyes. *Journal of American Chemical Society* 129: 5710-5718.

Smiley, S.T., Reers, M., Hartshorn, C.M., Lin, M., Chen, A., Smith, T.W., Steele, G. D., Jr., and Chen, L.B. 1991. Intracellular heterogeneity in mitochondrial membrane potentials revealed by a J-aggregate-forming lipophilic cation JC-1. *The Proceedings of the National Academy of Sciences (USA)* 88:3671-3675.

Smith, D.L. and Luss, H.R. 1972. The crystal structures of two solvates of 5,5',6,6'-tetrachloro-l,l',3,3'-tetraethylbenzimidazolocarbocyanine iodide. *Acta Crystallographica* B28:2793.

Soujanya, T., Saroja, G., and Samanta, A. 1995. AM1 study of the twisted intramolecular charge transfer phenomenon in p-(N,N-dimethylamino) benzonitrile. *Chemical Physics Letters* 236(4-5):503-509.

Waggoner, Alan S. 2005. Cyanine dyes as labeling reagents for detection of biological and other materials by luminescence methods. http://www.patentstorm.us/patents/6956032/fulltext.html (accessed June 10, 2008).

Wang, L.Y., Chen, Q.W., Zhai, G.H., Wen, Z.Y., Zhang, Z.X. 2006. Investigation of the structures and absorption spectra for some hemicyanine dyes with pyridine nucleus by TD-DFT/PCM approach. *Journal of Molecular Structure*: *THEOCHEM* 778:15-20.

Wang, L.Y., Chen, Q.W., Zhai, G.H., Wen, Z.Y., Zhang Z.X., 2007. Theoretical study on the structures and absorption properties of styryl dyes with quinoline nucleus. *Dyes and Pigments* 72:357-362.

Tomasi, J., Mennucci, B. and Cammi, R. 2005. Quantum mechanical continuum solvation models. *Chemical Reviews* 105:2999-3093.

Tomasi, J., Miertus, S., Scrocco, E. 1981.Electrostatic interaction of a solute with a continuum. A direct utilization of ab initio molecular potentials for the prevision of solvent effects. *The Journal of Chemical Physics* 55:117-124.

Young David. 2001. *Computational chemistry: a practical guide for applying techniques to real world problems*. John Wiley & Sons: United States of America.